Remote Sensing of Environment 204 (2018) 883–897

Contents lists available at ScienceDirect

Remote Sensing of Environment

journal homepage: www.elsevier.com/locate/rse

Utility of multitemporal lidar for forest and carbon monitoring: Tree growth, biomass dynamics, and carbon flux

Kaiguang Zhao[a,b,*], Juan C. Suarez[c], Mariano Garcia[d], Tongxi Hu[b], Cheng Wang[e], Alexis Londo[b]

[a] Ohio Agricultural and Research Development Center, School of Environment and Natural Resources, The Ohio State University, Wooster, OH 44691, USA
[b] School of Environment and Natural Resources, Environmental Science Graduate Program, The Ohio State University, Columbus, OH 43210, USA
[c] Forest Research, Northern Research Station, Roslin, Midlothian EH25 9SY, UK
[d] University of Leicester, Centre for Landscape and Climate Research, Department of Geography, Leicester LE1 7RH, UK
[e] Laboratory of Digital Earth Sciences, Institute of Remote Sensing and Digital Earth, Chinese Academy of Sciences, Beijing 100094, China

ARTICLE INFO

Keywords:
Multitemporal lidar
Repeat lidar
Biomass change
Individual tree
Tree growth
Carbon dynamics
Random forests
Scale
Model transferability
Bias

ABSTRACT

Lidar transforms how we map ecosystems, but its prospect for measuring ecosystem dynamics is limited by practical factors, such as variation in lidar acquisition and lack of ground data. To address practical use of multitemporal lidar for forest and carbon monitoring, we conducted airborne lidar surveys four times from 2002 to 2012 over a region in Scotland, and combined the repeat lidar data with field inventories to map tree growth, biomass dynamics, and carbon change. Our analyses emphasized both individual tree detection and area-based, grid-level approaches. Lidar-detected heights of individual trees correlated well with field values, but with noticeable underestimation biases ($r = 0.94$, bias $= -1.5$ m, $n = 598$) due to the increased probability of missing treetops as pulse density decreases. If not corrected for such biases, lidar provided unrealistic or wrong estimates of tree growth unless laser sampling rates were high enough (e.g., > 7 points/m^2). Upon correction, lidar could detect sub-annual tree growth (p-value < 0.05). At grid levels, forest biomass density was reliably estimated from area-based lidar metrics by both Random Forests (RF) and a linear functional model ($r > 0.86$, RMSEcv < 21 Mg/ha), irrespective of laser sampling rates. But RF constantly overfit the data, often with poorer predictions. The better generality of the linear model was further confirmed by its transferability—fitted for one year but applicable to other years—a strength not possessed by RF but desired to alleviate the reliance on ground biomass data for model calibration. Resultant lidar maps of forest structure captured canopy dynamics and carbon flux at fine scales, consistent with growth histories and known disturbances. The entire 20-km^2 study area sequestered carbon at a rate of 0.59 ± 0.4 Mg C/ha/year. Overall, our study describes robust techniques well suited for multitemporal lidar analysis and affirms the utility and potential of repeat lidar data for resource monitoring and carbon management; however, the full potential cannot be attained without the support of accompanying field surveys or modeling efforts in enhancing stakeholders' trustworthiness of lidar-based inference.

1. Introduction

Forests supply timber, shelter wildlife, store carbon, and regulate climate, among others (Bonan, 2008; Zhao and Jackson, 2014). Managing forests to sustain their benefits requires effective tools to monitor landscapes over time. Ground-based tools are valuable but with limited spatial footprints (West and West, 2009). This limitation has been addressed with the use of remote sensing, especially in meeting the growing demands for spatially-explicit forest maps to track forest loss and degradation and quantify terrestrial carbon pools (Goetz et al., 2015). Of current mapping technologies, airborne lidar features prominently, due to its superior ability to resolve 3D vegetation structure (Vierling et al., 2008). Since its advent, lidar has been often acclaimed as a breakthrough in the field of vegetation remote sensing (Babcock et al., 2015; Dubayah and Drake, 2000).

Over 50 years of research has demonstrated the utility of airborne lidar for natural resource assessment (Nelson, 2013). Existing lidar systems vary in laser type, footprint, data-recording, spectral specification, or operation mode (García et al., 2012; Shan and Toth, 2008). Our focus here is a most common system: small-footprint discrete-return single-band analog laser scanners (i.e., airborne laser scanning) or simply, airborne lidar. Empirical evidence continues to proliferate to prove the exceptional value of airborne lidar for measuring forest attributes and ecosystem structure with accuracies unattainable by its

* Corresponding author at: Ohio Agricultural and Research Development Center, The Ohio State University, Wooster, OH 44691, USA.
E-mail address: zhao.1423@osu.edu (K. Zhao).

http://dx.doi.org/10.1016/j.rse.2017.09.007
Received 19 September 2016; Received in revised form 17 August 2017; Accepted 10 September 2017
Available online 28 September 2017
0034-4257/

conventional counterparts (Coomes et al., 2017; García et al., 2015; Mutlu et al., 2008; Véga et al., 2016). Given its proven capabilities, the use of airborne lidar for 3D mapping is increasing rapidly around the world (Goetz et al., 2010; Zolkos et al., 2013). Many countries, such as Denmark, Finland, and Spain, even have national-level data acquisitions completed or in progress (Stoker et al., 2008), some of which are repeat surveys.

Increased use and availability of lidar data provide opportunities to measure and study ecosystem dynamics over time (Dubayah et al., 2010; Réjou-Méchain et al., 2015). This prospect is further boosted as lidar data costs are declining, data processing is becoming more standardized, and the lidar user base is expanding (Schimel et al., 2015; Stoker et al., 2008). Accompanying the prospect are also the increasing demands for high-resolution ecosystem dynamics products to address existing environmental challenges and emerging ecological questions (Asner et al., 2013; Ma et al., 2017). Current endeavors to map landscape dynamics are still dominated by the use of multi-date satellite imagery (DeVries et al., 2015)—an area that will benefit considerably from the use of multitemporal lidar. For instance, both satellites and airborne lidar have been emphasized as essential elements of carbon monitoring systems to measure, report, and verify carbon stocks and dynamics in support of REDD+ programs and forestry-based climate policies (Goetz et al., 2015).

Despite the widely envisioned potential of multitemporal lidar, practical implementations of lidar-assisted monitoring frameworks are limited (Dassot et al., 2011; Gatziolis et al., 2010; Srinivasan et al., 2014), urging for more case studies to exemplify multitemporal lidar analysis at multiple spatial scales for diverse forest types and conditions. Prior lidar vegetation studies focused mostly on a single time at a single scale, with only a limited number of lidar change studies (Ståhl et al., 2014). Cao et al. (2016), for example, identified only seven recent airborne lidar studies on biomass dynamics, all of which considered merely two points in time at grid/plot levels (e.g., Andersen et al., 2014; Hudak et al., 2012). Still, the use of repeat lidar data for tracking ecosystem changes across scales and beyond bi-temporal analyses is examined inadequately. Such multitemporal analyses seem to be simple extensions from single-time studies, but the extensions are not always straightforward with additional challenges involved, as highlighted next.

Effective use of multitemporal lidar data is affected by many practical factors, such as availability of ancillary ground data, variation in lidar acquisition, and choice of lidar analysis methods (Næsset, 2009; Zhao et al., 2011). Most area-based vegetation attributes, such as biomass and carbon density, cannot be measured by lidar directly. Instead, they are estimated from lidar metrics at grid cells empirically via correlative models, requiring paired ground-lidar data for model calibration (Næsset et al., 2005). This paradigm is typical of remote sensing retrievals of biophysical variables and is known to have issues with model generality and transferability: Models calibrated for one scenario—a given time, sensor, region, or modeler—are not applicable to another (Foody et al., 2003; Liang, 2007). Without spatially- and temporally-coincident ground data, calibration of lidar data is infeasible. This is particularly problematic for applications with historical lidar data where temporally-coincident ground data were not collected. Moreover, lidar technologies have been improving rapidly, and most repeat lidar data were acquired differently, for example, in terms of sensor, sampling rate, flight pattern, and collection date (Cao et al., 2016; Shan and Toth, 2008). Such inconsistencies further complicate multitemporal lidar analyses (Hirata, 2004; Næsset, 2009).

In addition to area-based vegetation analysis at grid levels, the ability of lidar to detect single trees is well documented (Li et al., 2012; Nunes et al., 2017; Popescu et al., 2003; Yu et al., 2006). Trees are often delineated using heuristic algorithms such as watershed segmentation and maximum filter (Zhao and Popescu, 2007). The algorithms vary in complexity but generally involve little or no use of ancillary ground data. Therefore, individual tree analyses have been believed to suffer less from those factors limiting grid-level analyses (Li et al., 2012). However, tree parameters obtained directly by lidar are distorted versions of true values. An example is the under-estimation of actual tree height, especially at lower laser pulse rates (Hirata, 2004; Popescu et al., 2003). Thus, these direct measurements still need to be corrected empirically. Some tree parameters, such as diameter, biomass, and age, cannot be directly measured by lidar and also need to be estimated empirically (Yu et al., 2011). As in grid-level analyses, individual tree analyses should also account for the many practical limiting factors, such as lack of ground data and varying lidar specifications. To date, lidar detection of individual tree growth over time remains largely unexplored.

This study aims to assess the utility of multitemporal lidar for tracking forest and carbon dynamics and tackle practical difficulties limiting the use of historical repeat lidar data for vegetation analysis. An emphasis is on evaluating and improving multitemporal lidar methods to measure forest changes over time at both individual tree and grid levels, including tree growth, canopy dynamics, biomass change, and carbon flux. We conducted four lidar surveys in 2002, 2006, 2008, and 2012, respectively, over a Scottish forest, collected field inventory data in 2002 and 2006, combined the data to quantify forest changes at either individual tree or grid levels, and more important, evaluated alternative modeling strategies to estimate biomass and carbon stock over time, especially if lacking temporally-concomitant ancillary data to calibrate lidar biomass models. Our analyses and results confirm the power of lidar for tracking forest changes and help to advance and encourage future use of repeat lidar for carbon monitoring and ecosystem dynamics studies.

2. Study area and data

Our study area is a 20 km^2 forested landscape near the Aberfoyle village (56°10′ N, 4°22′ W) in Scotland, UK (Fig. 1a). Part of the area falls within Queen Elizabeth Forest Park. Most of the area is covered with plantations, grown and clearfelled in 40 to 60 years' rotations, but ~10% of the forests are left to transition to a continuous cover forestry system. Forest stands are dominated by Sitka spruce (*Picea sitchensis* Bong. Carr), followed by other species such as European larch (*Larix decidua*), Norway spruce (*Picea abies* H. Karst), and Lodgepole pine (*Pinus contorta* Douglas). The area is characterized by a gentle topography. Windstorms are common in this region, with gusts peaking at 150 km/h and catastrophic wind events returning every 10 to 15 years.

Four airborne lidar datasets were collected for the study area over a ten-year span using Optech's ALTM sensors (Fig. 1b). The exact acquisition years are 2002, 2006, 2008, and 2012. Although similar sensors were deployed, the acquisition specifications of the four surveys differ from each other in terms of collection month, pulse repeat frequency, flying altitude, or sampling rate (Table 1). All the lidar surveys acquired both first and last returns. The 2006 data have the highest sampling intensity with an average point density of 23.7/m^2, followed by 8.1 for 2012, 6.1 for 2002, and 3.0 for 2008. Raw data were delivered by vendors as 3D discrete-return point clouds. Each return is also tagged with echo intensity, but only the xyz ranging data were considered for our analyses.

Field inventory data were first collected in 2002 on twelve 50 m × 50 m plots and again in 2006 on the same plots (Fig. 1a): no re-survey data for 2008 and 2012. Both field surveys were conducted shortly after the respective lidar flights to reduce temporal discrepancies. Established in 2002, the 12 plots were located across the region to capture the range of canopy variability (Fig. 1a). For ease of re-survey in 2006, four corners of each plot were marked with permanent posts and trees were numbered with metal tags. Tree parameters measured include dbh, height, crown width, and tree location. Dbh was tallied for all trees of > 7 cm in diameter. Tree height was measured with a Sonic Vertex III hypsometer for all trees in three 10 × 10 m^2 subplots selected inside each 50 m × 50 m plot as well as

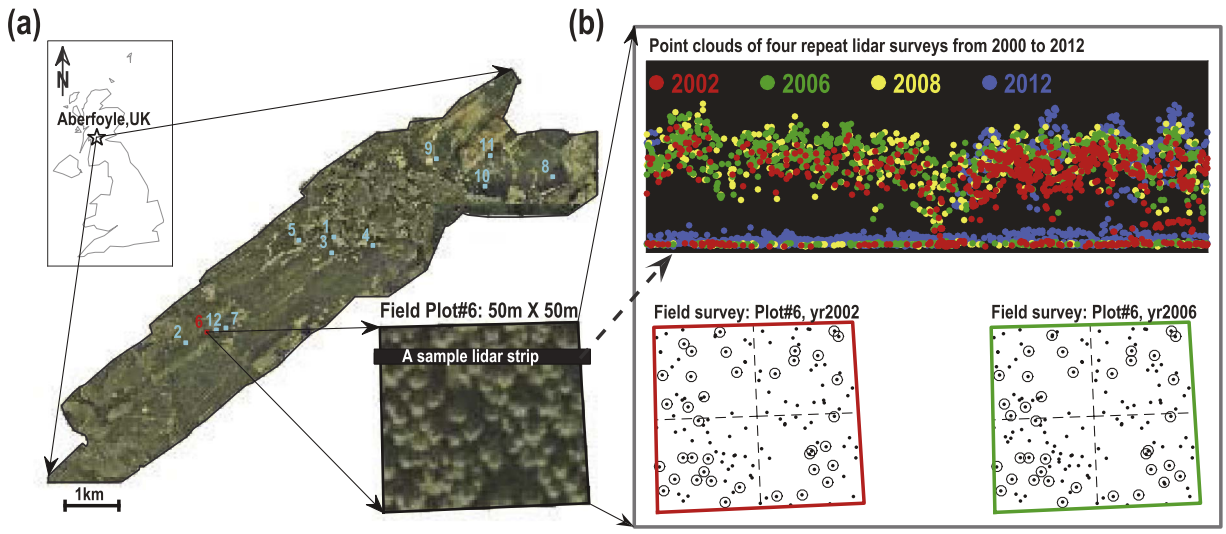

Fig. 1. (a) Study area and (b) availability of field and lidar data. Twelve 50 m × 50 m field plots were surveyed in both 2002 and 2006. Four repeat lidar surveys were flown in 2002, 2006, 2008, and 2012, respectively, capturing forest changes over time (Upper B).

for a fraction of randomly selected trees across each plot. Tree locations were obtained using a Leica 500 DGPS and a Trimble 5600 total station: Near each plot, some reference points were first selected as ground stations, the coordinates of which were obtained by integrating 20 min's GPS signal; then the GPS coordinates were combined with the total station readings to compute tree locations via triangulation.

3. Methods

We combined the lidar and field data to derive forest parameters for each of the four lidar surveys and examine their temporal changes. An overview of our analyses is depicted in Fig. 2, including a set of data processing, algorithms, and correlative modeling that vary in nature and complexity. We considered two levels of spatial unit: individual trees vs. grid cells (i.e., plots). These are common analysis units chosen for routine use of lidar (Coomes et al., 2017). Specifically, our individual tree analysis aims to measure changes in tree height (Fig. 2). We implemented a customized algorithm to delineate trees, corrected the relative biases of lidar-measured tree heights associated with the differing pulse densities, and applied a semi-automatic scheme to match trees of different sources. At grid levels, we computed various lidar metrics, classified spatiotemporal patterns in forest change, and evaluated multiple modeling strategies to estimate biomass and carbon dynamics. Below, we elaborated on the approaches for three groups of analyses (Fig. 2): lidar data processing, individual tree analyses, and grid-level analyses.

3.1. Lidar data processing

Raw lidar point clouds were converted into several intermediate products, such as DEM, normalized point clouds, and canopy height model (CHM) (Fig. 2, top). In brief, we first classified the raw lidar point cloud of each survey to separate ground from non-ground points, using an iterative TIN-based method developed by Axelsson (2000). Ground points classified were then interpolated into DEMs at a 0.5 m resolution. The DEM quality was checked in reference to ten independent GPS control points, showing an overall RMSE of 6.3 cm. Next, DEMs were subtracted from the raw point cloud, yielding a detrended point cloud that has a ground elevation of zero and captures canopy vertical structure. The detrended data, known as normalized point cloud, were used to compute area-based lidar metrics and were also rasterized into CHMs at a 0.25-m resolution by tri-angulating and interpolating local-maxima points of the cloud. These processing steps yielded intermediate lidar products essential for the subsequent lidar forest analyses (Fig. 2).

3.2. Individual tree analysis: tree delineation

Our individual tree analysis focuses on tree height and its dynamics. To isolate individual trees and measure tree height, we implemented a lidar delineation algorithm based on maximum filtering and watershed segmentation. First, a circular variable-window maximum filtering was applied to the lidar CHM, identifying local maxima as treetops (Fig. 2, lower left). The filter window mimics a moving crown. Its size increases with height, varying adaptively according to an equation fitted from our field-measured crown width (CW, meter) and height (H, meter):

Table 1
Four lidar datasets and associated acquisition specifications. Note that data costs were adjusted for inflation to 2012 pounds and lidar ranging errors are the manufacture's nominal values that were found consistent with our independent accuracy estimates based on the error propagation method of May and Toth (2007).

Year	2002	2006	2008	2012
Sensor	Optech ALTM2033	Optech ALTM2100	Optech ALTM2100	Optech Gemini 167 ALTM
Date	19 Sept. 2002	31 May 2006	12 Mar. 2008	31 Mar. 2012
Laser pulse frequency	33,000 Hz	100,000 Hz	100,000 Hz	100,000 Hz
Flying altitude	1000 m	950 m	1000 m	1000 m
Beam divergence	0.3 mrad	0.3 mrad	0.3 mrad	0.3 mrad
Scanning angle	20°	10°	20°	10°
Average point density	6.1 pts/m^2	23.7 pts/m^2	3.0 pts/m^2	8.1 pts/m^2
Nominal vertical accuracy	5–10 cm	5–10 cm	5–10 cm	5–10 cm
Nominal horizontal accuracy	10 cm	9 cm	10 cm	10 cm
Acquisition cost	6.5£ per ha	6.1£ per ha	1.2£ per ha	1.0£ per ha

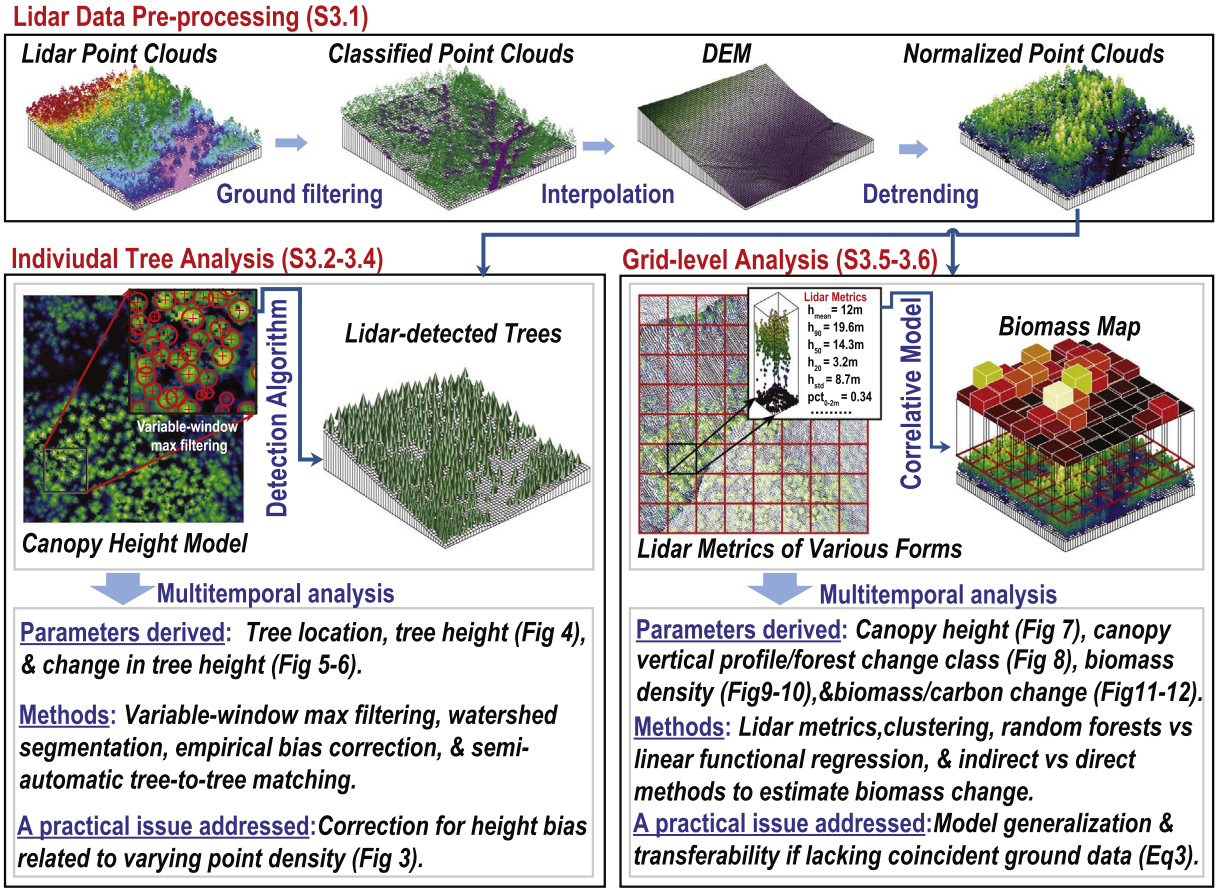

Fig. 2. Derivation of forest parameters at two contrasting analysis-unit levels—single tree vs. grid. Raw 3D point clouds were first filtered and detrended to obtain terrain and canopy. Then, detrended point clouds were rasterized into canopy height model for individual tree delineation using a customized single-tree algorithm and were also gridded into lidar metrics to estimate canopy parameters (e.g., biomass & carbon) at chosen spatial resolutions via correlative modeling, providing a methodological basis for multitemporal lidar analysis.

$CW = 0.7 + 0.084H - 0.001 * H^2$. This lidar filter was proposed by Popescu et al. (2003), and its efficacy is substantiated by the fact that for many species, higher trees have larger crowns and tree apexes are locally highest. We considered the horizontal coordinates of identified treetops as tree xy locations. Second, the treetops were treated as markers to initiate a watershed segmentation of the CHM, analogous to pouring water into the inverted CHM (Zhao and Popescu, 2007). Each tree marker led to a tree "basin" that holds the tree crown, which provided a mask to clip out the lidar points falling within it. The maximum z-value of the clipped point clouds was computed and used as lidar-measured tree height.

3.3. Individual tree analysis: tree-to-tree matching

We next applied a semi-automatic method for matching trees to trees. The matching is needed between field and lidar trees so as to perform accuracy assessment as well as between lidar trees of different years so as to calculate tree growth. Given two sets of treetops (i.e., points), say A and B, any point in A can find a closest point in B, and vice versa, but the identified point in B has a closest point back in A that is not necessarily the original A point. This asymmetry is similar to the concept of Hausdorff distance and can be leveraged to help to pair treetops. Specifically, we paired a point in one set to another point in a second set, if and only if the two points are the closest points to each other—a rule originally explored by Yu et al. (2006). Moreover, in the matching, the point-to-point distance measure is not necessarily confined to horizontal planimetric distance but rather can be any distance metric. The particular distance metric we used accounts for both horizontal locations (i.e., x, y) and height (h) such that the metric distance of any two treetops—(x_1,y_1,h_1) and (x_2,y_2,h_2)— is

$$D = \sqrt{\underbrace{(x_1 - x_2)^2 + (y_1 - y_2)^2}_{\text{planimetric distance}} + w \cdot \underbrace{(h_1 - h_2)^2}_{\text{height diff}}} \quad (1)$$

where the user-specified parameter w weights the vertical height difference against the horizontal distance; here a value of 0.5 was used for w as a simple, empirical choice.

With the distance metric of Eq. (1), we ran the above matching method to automatically obtain a preliminary list of paired trees. As a further step, when matching between field and lidar trees (e.g., for 2002 or 2006), we followed the manual procedure described by Popescu and Zhao (2008) to visually check through the automatic pairs in a GIS and rectify the mismatching or simply remove the uncertain ones. When matching lidar trees among the four lidar acquisitions, we kept only those of the automatic matched trees that are present in all the four years and that do not show a decrease in height by a selected threshold (i.e., 3 m as chosen here). This heuristic rule was elicited by observing that trees seen in one year may disappear in a later year due to mortality or logging and trees are unlikely to dramatically shrink in height over time. Overall, our semi-automatic tree-matching procedure was designed to minimize the commission error, though at the cost of increasing the omission error.

3.4. Individual tree analysis: correction for bias in tree height

More importantly, we evaluated how the lidar-measured individual tree height would vary under differing laser sampling/point intensities and then modeled the height-sampling intensity relationship as a way to empirically correct for lidar underestimation biases (Fig. 3). Tree

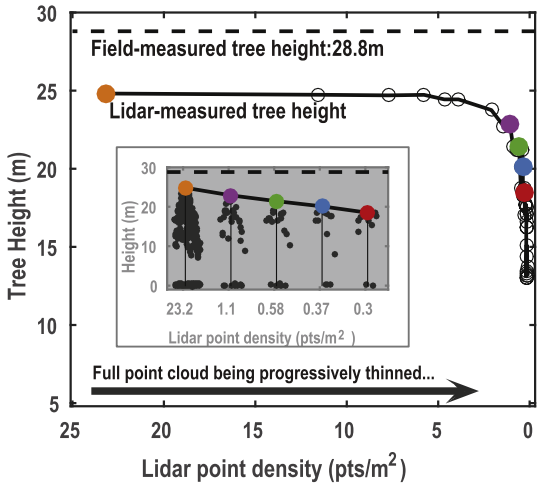

Fig. 3. Quantifying the dependence of lidar-measured tree height on lidar point density as a way for bias correction: Lidar tends to miss treetop and underestimate true tree height, especially at lower lidar point densities. Shown here is an example tree measuring 28.8 m in the field that was sampled with 23.2 points per m^2 by lidar in the year 2006. Its original lidar point cloud was progressively thinned into lower-density data (e.g., the inset), serving a proxy dataset to infer an empirical bias-lidar point density relationship.

heights calculated in Section 3.2 are known to underestimate actual heights because lidar tends to miss treetops (Hirata, 2004; Sibona et al., 2016): The magnitudes of the underestimation are not constant but vary with lidar point density (Fig. 3). The lower the point density is, the larger the underestimation bias. Our four lidar surveys have different sampling rates (Table 1); even for the same survey, lidar point densities varied across the scenes. If not corrected for the density-dependent biases, then estimates of tree growth—the difference in height between two years—will be incorrect because the biases for the two years do not necessarily cancel out on their own.

To quantify and correct such biases pertinent to lidar sampling rate, we chose the 2006 lidar data—the acquisition with the highest laser pulse rate and thinned it at a series of lower point densities (Fig. 3). These multiple low-density versions of lidar data allowed us to generate a series of lidar-measured heights under the differing point densities for the same tree (Fig. 3). The varying tree height (H) as a function of point density (PD) was fitted using a model parameterized by H_0, a, b, and c:

$$H = H_0 - a \cdot \exp(-b \cdot PD^c) \quad (2)$$

which permits determining the change in bias of individual tree height for variation in lidar point density. Eq. (2) is an empirical model fitted merely from the lidar data (Fig. 3); it doesn't necessarily encode the information on absolute bias (i.e., the difference of lidar height from its true unknown value). Therefore, our use of Eq. (2) was intended primarily for correction of relative biases: The correction for the relative bias between two point densities PD_1 and PD_2 for a tree is simply $a \cdot [\exp(-b \cdot PD_1^c) - \exp(-b \cdot PD_2^c)]$. We fitted the relationships in Eq. (2) from the 2006 data separately for each individual tree and applied the tree-specific relationships to empirically correct for height biases of the other three years relative to the 2006 baseline data.

3.5. Grid-level analysis: change in canopy structure

In addition to the analysis of individual-tree height dynamics, we analyzed the lidar data to characterize forest structural changes at grid levels across the landscape by examining two common area-based lidar metrics: canopy height and canopy height profile (CHP). First, canopy height is defined here as the mean height of canopy top surfaces over a grid and was calculated by simply aggregating the 0.25-m CHM to a 5-m resolution. The choice of 5 m represents a tradeoff between retaining spatial details and suppressing subgrid heterogeneity due to random canopy architecture. Unlike other lidar metrics such as percentile and maximum heights, the canopy height metric so calculated is an unbiased estimator of mean canopy height independent of lidar sampling rates (Thomas et al., 2006; Zhao et al., 2011); therefore, no correction for relative biases was performed in our grid-level comparison of canopy height among the four data years.

Second, our CHP metric is analogous to lidar waveform and is a composite metric that depicts the vertical variability of canopy structure with height. As in Popescu and Zhao (2008), we derived it by counting the relative vertical distribution of lidar points within each voxel for a number of height bins at a given grid. The grid size should be sufficiently large to contain enough lidar points and was set here to 25 m. The vertical range we chose is from the ground to an upper limit of 35 m, divided into 35 bins at a 1-m interval. Thus, each CHP is a discretized curve consisting of 35 normalized density values. Other authors may compute CHP in slightly different ways (e.g., Næsset et al., 2005; Palace et al., 2015). Regardless, CHP used here is equivalent to canopy density metrics or lidar height-bin data explored in these earlier studies.

For our grid-level change analyses, canopy height and CHP were treated differently. Canopy height is a single raster layer for each year. Therefore, changes in canopy height between any two years were calculated as pixelwise differences; their temporal trajectory for pixels can be easily visualized and interpreted. In contrast, CHP is hyperspectral-like data, comprising 35 bands, and can be analyzed in numerous ways to leverage this information-richness. Here, to identify spatial patterns of forest changes, we stacked the four years' CHP data, resulting in a total of 140 layers, and then clustered the stacked layers into ten forest change classes with the k-means algorithm. We also created volumetric rendering of the CHP data to aid in visual interpretation.

3.6. Grid-level analysis: biomass dynamics and carbon fluxes

Biomass and its change were estimated via correlative modeling by seeking empirical regression models to relate field-based biomass with lidar metrics (Fig. 2). To obtain field-based reference biomass for fitting and testing regression models, we divided each of the twelve 50 × 50 m plots into four 25 × 25 m quarter plots (Fig. 1b), yielding a total of 48 data points. Field-based biomass on each quarter plot was computed by aggregating tree total biomass—including both belowground and aboveground components—estimated from the combination of field dbh measurements and general species-specific allometry equations (Green et al., 2007; Muukkonen, 2007). Given the field-based biomass, the model fitting then reduces to determining what lidar metrics and model forms should be used—a process informed by not just strengths of modeling techniques but also subjective knowledge.

We considered two model techniques: the Random Forests algorithm (RF) (Friedman et al., 2001) and a semi-mechanistic linear functional model (Zhao et al., 2009). The two differ in principle and require different types of lidar metrics as predictors. RF is a general-purpose machine learning technique capable of approximating complex relationships with decision trees. Its use for remote sensing applications is growing. Its effectiveness is supported both empirically and theoretically, especially due to its reliance on not just one decision tree but an ensemble of trees (e.g., hundreds or thousands) as a strategy to improve model robustness. Similar to the machine learning-based analysis of Zhao et al. (2011), the lidar metrics we chose here for RF consist of 52 common metrics, including quantile heights, canopy densities, mean height, and standard deviation and coefficient of variation of lidar heights.

Our second choice—the linear functional biomass model—was originally proposed by Zhao et al. (2009). The model features some unique advantages. It is scale-invariant, that is, calibrated for one plot size or shape but applicable to another without introducing artificial discrepancies. Its model form was derived from first principles, mathematically relating canopy height distribution (CHD) to biomass density.

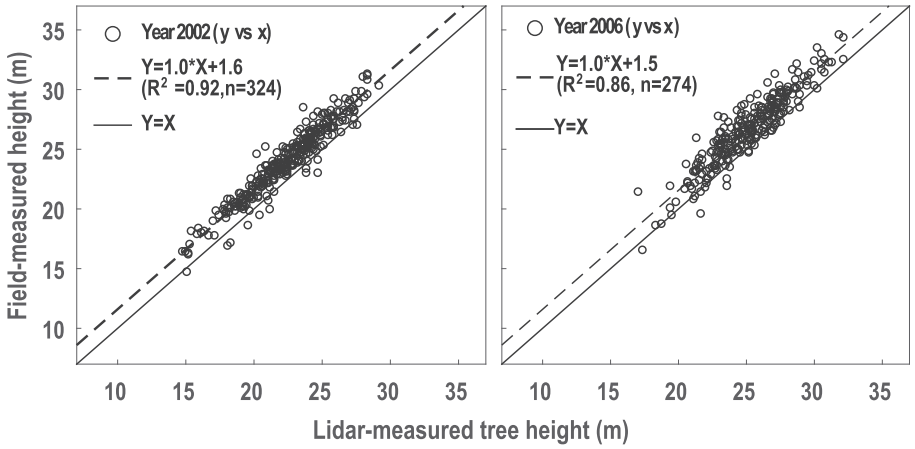

Fig. 4. Comparisons of field and lidar heights of individual trees for year 2002 (left) and 2006 (right).

For this reason, we term it as a semi-mechanistic model. Our so-called CHD resembles but differs fundamentally from the canopy height profile (CHP) of Section 3.5. On a given grid, CHP captures the vertical variability of the whole vertical canopy layer, including within-crown materials. But CHD, denoted by $p(h)$, is defined here as the height variability of top canopy surfaces only—the outer envelope of crowns and exposed ground. The discretized version of CHD, $p_{i=1,\ldots,n}$, was computed as a histogram of canopy height for each 25 m × 25 m grid from the lidar CHMs, with n being the number of histogram bins; then CHD is related to biomass via

$$\begin{aligned} Biomass &= f(p_{i=1,\ldots,n}) \\ &= \int k(h)\cdot p(h)\mathrm{d}h \xrightarrow{\text{discretized by}\Delta h} \Delta h\cdot \sum k_i\cdot p_i \end{aligned} \quad (3)$$

where $k(h)$ or its discretized version $k_{i=1,\ldots,n}$ is a non-decreasing function of height h. Eq. (3) is a functional or curve regression model because the predictors are not just a few metrics but a curve $p(h)$ (Magnussen et al., 2016). After the discretization, Eq. (3) is linear with $k_{i=1,\ldots,n}$ being the unknown coefficients to be estimated from the training data. Unlike most of the empirical models previously examined, the model in Eq. (3) is theoretically justified (Zhao et al., 2009) and it has the potential to infer a lidar-biomass relationship that is generalizable and transferrable—a feature tested here based on our 2002 and 2006 data.

To assess and compare the RF and linear models, we applied three evaluation strategies. Foremost, we capitalized on the availability of both 2002 and 2006 field data to test the models' generalizability and transferability: We fitted models from data of one year and tested them against data of the other year. The testing of model generality is critical for our biomass change analysis. Only if the model generality is confirmed, can we safely apply the lidar biomass models calibrated upon the 2002 and 2006 data to estimate biomass in the years 2008 and 2012 for which we lack ground data to calibrate their own year-specific models. Second, we evaluated models based on diagnostic statistics from model calibration, but such statistics are not robust indicators of predictive power, partly because machine learning models like RF have high expressive power and may fit data arbitrarily well. Models can be more reliably evaluated using out-of-training-sample data. Accordingly, we performed the leave-one-out cross-validation as our third way to assess models.

We also compared indirect and direct methods to estimate biomass change between the years 2002 and 2006. The indirect method estimates the change ΔB by first fitting two different models, $f_{06}(\cdot)$ and $f_{02}(\cdot)$, to predict biomass separately for each year and then taking difference $\Delta B = f_{06}(\text{lidar}) - f_{02}(\text{lidar})$. The direct method fits just one model $f_{06\_02}(\cdot)$ that directly relates biomass difference to lidar metrics, $\Delta B = f_{06\_02}(\text{lidar})$. More generally, when estimating pairwise biomass differences among N years, the indirect method will fit only N models, one for each year, but by the combinatorics, the direct method needs to fit $N*(N-1)/2$ models, one for each pair of two chosen years.

Finally, we calculated carbon flux, defined here as the rate of change in forest carbon stock. Carbon stock, including both standing and root biomass, was simply converted from lidar-derived biomass density using a generic scaling factor of 0.5 (Englhart et al., 2013); therefore, carbon flux was obtained as the change in total tree biomass per unit area per year, scaled by 0.5. Positive carbon fluxes indicate sinks associated with carbon accumulation from natural growth, and negative fluxes are carbon sources due to various disturbances.

4. Results

4.1. Individual analysis: tree height and growth

Lidar-measured tree heights correlated strongly with field values (r = 0.96 for 2002 and 0.93 for 2006), but with noticeable underestimation biases (Fig. 4). The comparison was made based on all the matched field and lidar trees. In our field surveys, 490 and 395 trees were tallied for height in 2002 and 2006, respectively. For the 2002 data, only 354 of the 490 field trees were paired to lidar-detected trees by our automatic tree-to-tree matching – a rate of 72%. Not all the matches were correct; as the second step of our semi-automatic method, a manual check showed that 30 of the 354 matches were commission errors. For the 2006 data, 302 of the 395 field trees (76%) were automatically paired to lidar trees, with 28 pairs being mismatches. Comparisons between these correctly-matched trees showed that lidar underestimated field tree height by 1.6 m in 2002 and 1.5 m in 2006 (Fig. 4).

The degree to which lidar underestimated height depended on lidar point densities. The dependence was reliably quantified by our empirical correction model at individual tree levels. Applying the empirical correction improved estimation of tree height and growth (Fig. 5). Using the single tree in Fig. 3 as an example, its lidar-detected height was found to decrease as the lidar data were progressively thinned, showing larger underestimation biases at lower point densities. This relationship was modeled well by our parametric equation of Eq. (3), $H = 24.8 - 39.2*\exp(-2.8*PD^{0.372})$ ($R^2 = 0.90$), and was used to correct height biases. When evaluated upon the 2002 and 2006 field trees, the bias correction helped to reduce the RMSEs of lidar-measured tree heights from 1.53 m to 0.11 m (n = 598).

If not applying such empirical corrections, the tree growth from 2002 to 2006—difference in tree height—was correlated to the field estimation weakly, with a correlation coefficient of r = 0.34 based on 224 pairs of trees matched between 2002 and 2006 plus between lidar and field trees (Fig. 5). The bias correction increased the correlation from 0.34 to 0.67 and reduced the overall bias from −0.27 m to 0.02 m

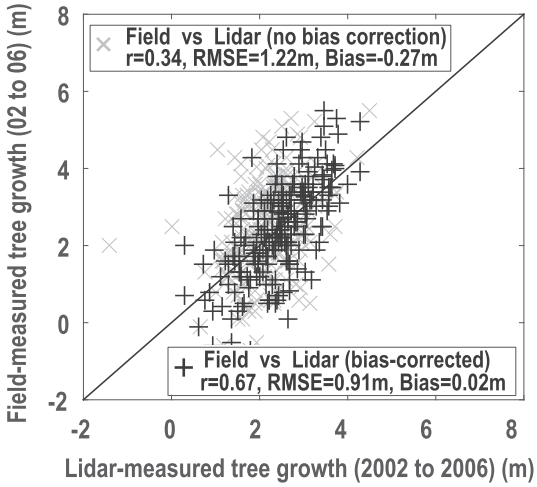

Fig. 5. Comparisons of field-measured and lidar-derived tree growth from 2002 to 2006 (n = 224 trees). The 2002 and 2006 lidar data were acquired at different sampling rates and thus underestimate tree height differentially (see Fig. 3). Growth estimates by taking direct differences are therefore still biased (depicted as crosses); correction for the biases using the method illustrated in Fig. 3 helped to improve estimation of tree growth (pluses).

(Fig. 5). Our empirical correction model also suggests that if lidar point densities go beyond certain thresholds (e.g., ~7 pts/m^2), the biases become insignificant and thus, no correction is needed.

Trajectories of tree growth from 2002 to 2012 were captured well by lidar, but only if we corrected for the height biases associated with the varying lidar point densities (Fig. 6). The 2008 lidar data have the lowest point density and appeared to underestimate tree height most severely (Fig. 6, left). If not bias-corrected, the estimated growth was unreasonable and in many cases, wrong (Fig. 6, left): Trees shrunk in size over time, contradicting the fact. In contrast, the trajectories corrected for the point density effect clearly revealed linear or sigmoid growth, consistent with the known stand growth histories in this region. These growth trends were observed at both individual tree and plot levels (Fig. 6).

Upon correction for the density-related biases, lidar was able to detect short-term individual tree growth, even at a sub-annual scale. Based on a comparison of lidar-detected and field-measured tree growth from 2002 to 2006, the uncertainty in lidar-derived tree growth was estimated to be 0.24 m/year (i.e., SE). Meanwhile, by fitting a line to the mean growth trajectories of 3400 lidar-detected trees over the field plots (Fig. 6), we estimated the overall tree growth to be 0.62 m/year from 2002 to 2012. The combination of the two estimates implies that annual tree growth is detectable by lidar with a probability of 96.5%. Put it differently, our repeat lidar surveys should be at least 0.46 year apart to be able to detect individual height change at a 95% confidence level. The practical interpretation of this resolving ability, however, needs to account for non-uniform tree growth within a year.

4.2. Grid-level analysis: change in canopy structure

Beyond the individual tree level, changes in canopy height were measured well by lidar across the landscape and over time. In Fig. 7, the maps of pairwise differences in canopy height depict fine-scale forest height dynamics at a 5 m resolution for a 1 km × 1 km subset of the study area over the ten years. The height dynamics for all the 40,000 pixels in this subarea was also synthesized in the density plot in Fig. 7, depicting multiple distinct groups of trajectories that correspond to different stand management activities and disturbance regimes. In the lidar maps, stands of varying age classes were distinctly noticeable. Mature tall stands were seen to be clearfelled over the 10 years, although portions of tall forest stands were left unlogged and managed as a continuous cover forestry system. Some patches of low-stature stands were also found to be removed; these patches were heavily damaged by a wind storm in January 2005. Such tree losses from the gales were also noted from the 2006 field survey near Plot 1, 3, 4, and 5. All these management activities and windthrow were observed and spatially delineated by multitemporal lidar. For those patches less disturbed, the lidar data captured natural growth and gap dynamics (Fig. 7). The growth partially compensated for the canopy losses from the disturbances; the overall trend over the 10 years was still a decline in mean canopy height for this 1 km × 1 km area (Fig. 7).

Changes in 3D canopy structure were captured vividly in the canopy height profile (CHP) data (Fig. 8a). The volumetric view of stacked CHP in Fig. 8a offers a tomography-like depiction of within-canopy

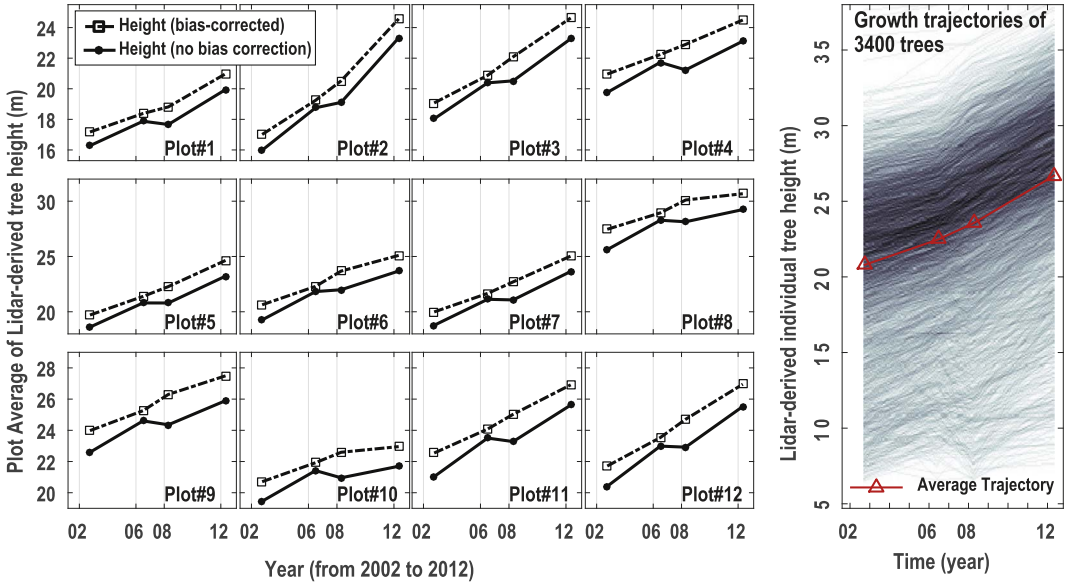

Fig. 6. Lidar-derived tree growth from 2002 to 2012 for the 12 plots, as depicted for each plot separately (left panel) or in combination (right panel): Lidar gave unreasonable growth trajectories if not corrected for the relative biases caused by the varying lidar sampling densities over years (filled circle), compared to the trajectories corrected for the biases (open square). The density plot on the right is a heatmap-like visualization of the assembled growth trajectories of 3400 trees in the height-time space wherein darker areas indicate higher occurrences of trajectories passing through.

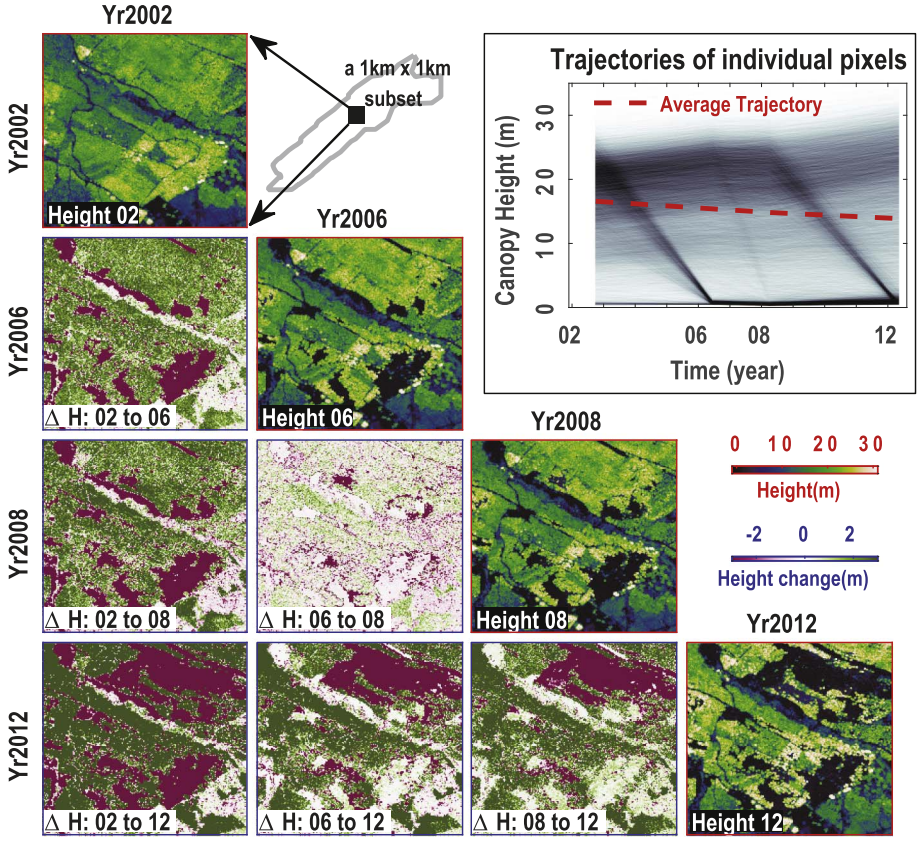

Fig. 7. Changes in lidar-derived forest canopy height for a 1 km × 1 km subregion at a 5 m grid resolution through 2002–2012. The four diagonal images refer to canopy height for the four data years whereas the images on the lower triangle refer to height differences between any two of the four years. On the upper right, the density plot depicts the assemblage of trajectories for the 40,000 pixels of this subregion: Two clusters of sloping-down trajectories are distinct, corresponding to those forests logged between 2002 and 2006 and between 2008 and 2012, respectively.

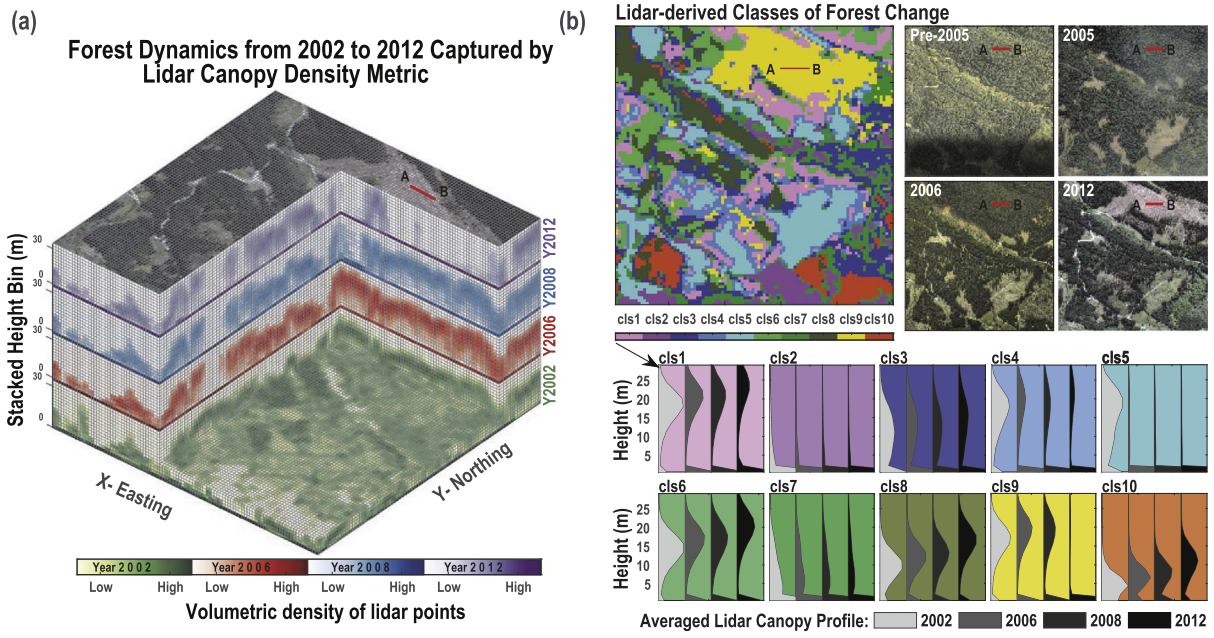

Fig. 8. Forest structure changes over time on the 1 km × 1 km region of Fig. 7. (a) A 3D volumetric view of lidar canopy height profiles stacked vertically for the four years. Darker colors denote higher lidar point densities, namely more plant materials. (b) The stacked 3D height-bin data were classified into ten forest change classes (top), which show distinct canopy height profiles (bottom). Juxtaposed to the upper right are four Google Earth photos. A line segment "AB" of 100 m in length is drawn as a reference of scale. (For interpretation of the references to color in this figure legend, the reader is referred to the web version of this article.)

structures in a 3D voxel-based space. The amount of phytoelements in each voxel is indicated by the relative number of lidar echoes falling within it. Open voxels, therefore, are locations devoid of canopy materials. Examples of such relatively open voxels are the sparse understory of tall mature sitka spruce stands and those newly cleared stands (e.g., the stand labeled the by segment AB in Fig. 8). The rich information inherent in the CHP data was leveraged to classify spatial patterns of forest change (Fig. 8b). The resulting ten classes have spatial distributions resembling stand boundaries and management patterns. The mean CHPs averaged over each class for each year, as plotted in Fig. 8b, further reveal the distinct patterns in canopy growth and vertical structure. For example, Class2 are open corridors devoid of tall

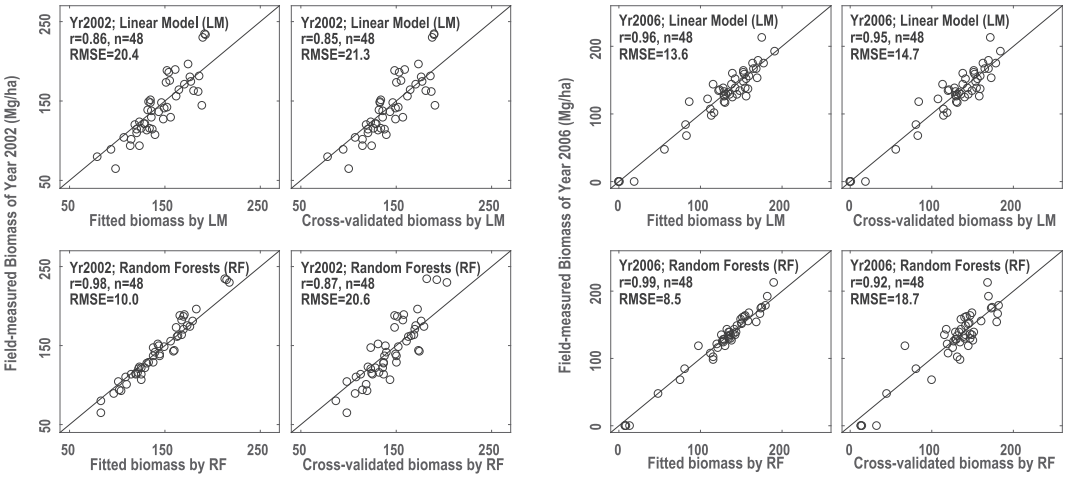

Fig. 9. Comparisons of in-situ and lidar-estimated biomass for year 2002 (left) and 2006 (right) using either linear functional model (LM, top) or Random Forests (RF, bottom). RF fitted data better but didn't necessarily yield better prediction accuracies in cross-validation; that is, RF overfit the data and LMs had better predictive power and generalization.

trees throughout the ten-year period; Class5 are those forest stands cleared sometime between 2002 and 2006; and Class10 are low-stature stands that remained undisturbed and kept growing from 2002 to 2012.

4.3. Grid-level analysis: biomass density and carbon flux

Lidar-estimated biomass densities agreed well with field estimates for either the year 2002 or 2006 (Fig. 9). Of the two estimation methods, random forests (RF) constantly overfitted the data but the linear functional model (LM) didn't. For example, for the year 2006, RF fitted the data tightly, with a RMSE of 8.5 Mg/ha compared to 13.6 Mg/ha from the LM fitting (Fig. 9, right). The better fitting (i.e., calibration) may misinform practitioners of the better predictive power with RF. A more reliable testing via the leave-one-out cross validation indicated otherwise. The RMSEs from the cross-validation are 18.7 mg/ha for RF and 14.7 ma/ha for LM. These cross-validation statistics are better indicators of the true predictive powers than are the model statistics from the model calibration phase. The consistency of diagnostic statistics (e.g., RSME) between model calibration and validation suggests that LM has better generality (Fig. 9) and is more likely to capture the true empirical relationship between biomass and lidar metrics, but this consistency was not observed for RF.

The superior generality of LM was further confirmed by its demonstrated model transferability. That is, LM fitted from data of one year is applicable to make predictions for another year (Fig. 10). For example, the LM fitted from the 2002 training data was applied to the 2006 data, producing an average predictive error of 15.7 Mg/ha for the 2006 biomass. This error is statistically the same as that obtained by using the LM directly fitted to the 2006 data (14.7 Mg/ha). Likewise, the LM fitted to 2006 data was equally applicable to predict 2002 biomass using the 2002 data (Fig. 10, left). This transferability suggests that LM captures a general time-invariant functional relationship between biomass and lidar metrics. In contrast, the model transferability of RF was much poorer (Fig. 10, bottom).

Lidar estimates of biomass change from 2002 to 2006 were predicted with reasonable accuracies using both the indirect and direct methods (Fig. 11). The overall error of lidar-estimated rate of change was 5 Mg/ha/year, as assessed against field-based estimates. Of the two methods examined, we found that the indirect method, where the change is calculated as the difference between 2002 and 2006 biomass estimates, showed slightly better performances (e.g., $RMSE_{indirect}$ = 17.2 vs. $RMSE_{direct}$ = 19.4 Mg/ha) (Fig. 11). To many practitioners, such a gain may be practically marginal. More important, if pairwise changes need to be computed for N years, the indirect method will fit N models. But the direct method will fit a total of $N * (N - 1) / 2$ models plus it requires repeat field surveys for exactly the same plots through the n years to obtain field-based biomass differences—a stringent constraint for many practical applications. Irrespective of the indirect or direct method, the use of LM improved the prediction of biomass change over the use of RF (Fig. 11).

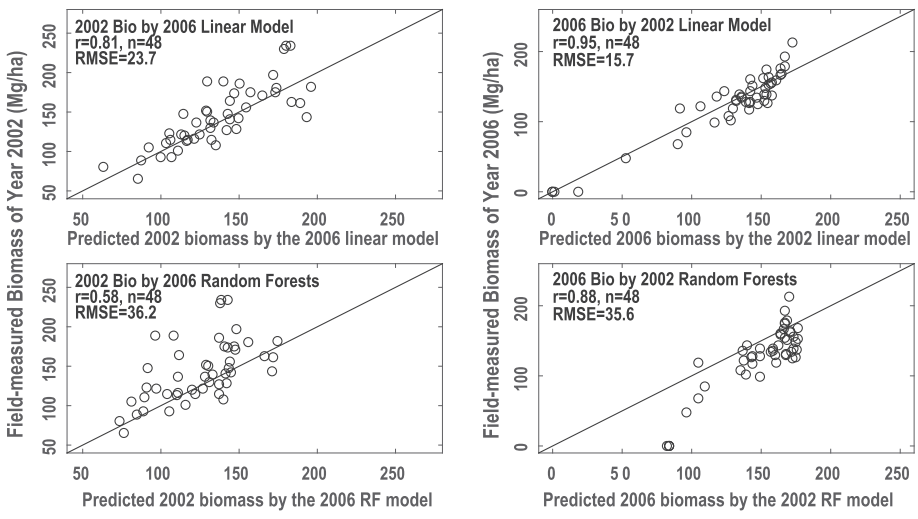

Fig. 10. Comparisons of in-situ and lidar-predicted biomass. Unlike Fig. 9 where models were fitted and applied to the same dataset of a chosen year, here models were fitted from data of one year and then applied to independent data of the other year. As in Fig. 9, linear models outcompeted random forests. Linear models showed better generality and were transferrable from one time to another.

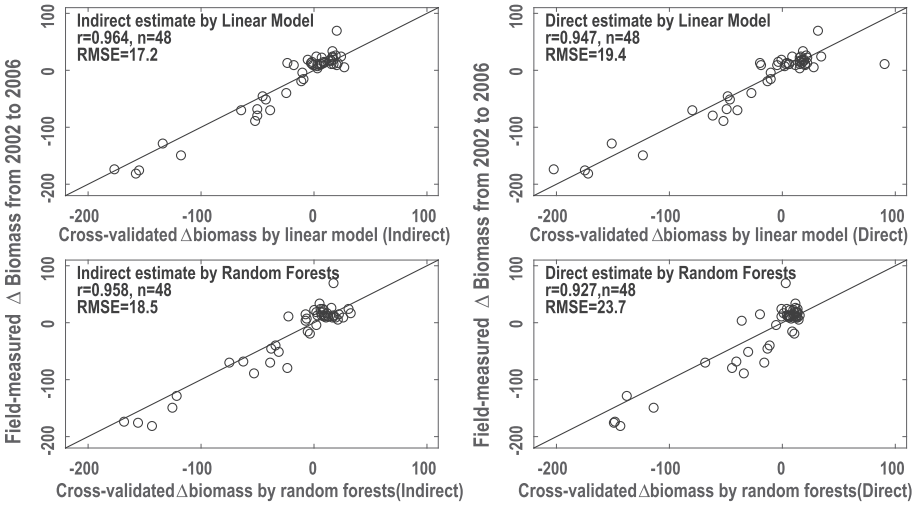

Fig. 11. Scatterplots of in-situ vs. lidar-predicted biomass changes (2002 to 2006) that were estimated using either indirect methods $\Delta B = f_{06}(\text{lidar}) - f_{02}(\text{lidar})$: estimate biomass for the two years separately and then take difference or direct methods $\Delta B = f_{06\ -\ 02}(\text{lidar})$: estimate biomass difference directly from a single model. Indirect estimates were slightly more accurate than direct ones. Linear models outcompeted random forests for both indirect and direct methods.

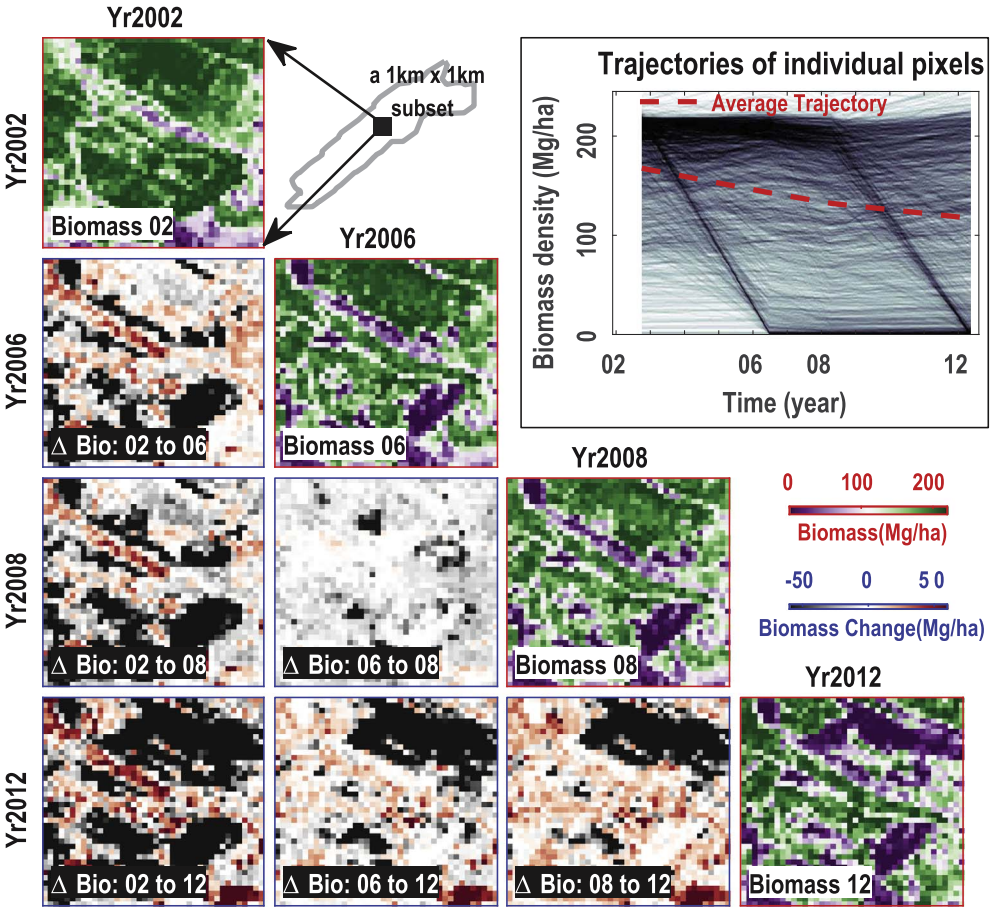

Fig. 12. Changes in biomass density over time for a 1 km × 1 km subregion at a 25-m resolution. Biomass was all estimated using the linear functional model through years. Four diagonal images refer to biomass density for the four data years. The images at the lower triangle refer to biomass change from one year to another, wherein black patches correspond to carbon sources and reddish patches to carbon sinks. Shown on the upper right is a density plot of biomass trajectories of 1600 pixels. The average trajectory shows an overall decline in carbon stock, with an estimate loss of −2.63 Mg C/ha/year.

The validated generality and transferability of our linear functional model allowed us to safely apply it to estimate biomass for all the four years. We have field survey data for only 2002 and 2006 not for 2008 and 2012. Thus, we fitted a LM from the combined 2002 and 2006 training data, and used it as a generic model to predict biomass and carbon for the four years at a 25-m resolution. The mean forest biomass density averaged over the entire 20-km^2 region is 63.3, 69.0, 72.5, and 74.5 Mg/ha for the four years, respectively, acting as a carbon sink with a rate of 0.59 ± 0.4(SE) Mg C/ha/year. The landscape at finer scales showed distinct spatial patterns in biomass density and carbon fluxes (Fig. 12). The fine-scale heterogeneity is known to be driven by local management practices and natural distances and was depicted in the 25-m lidar maps. For the same 1 km × 1 km area as in Figs. 7 & 8, patches of major carbon sink and carbon source clearly coincide with the boundaries of stands and management units, losing carbon at a rate of 2.63 Mg C/ha/year (Fig. 12). The carbon footprint from the 2005 windstorm was also visible in the map of biomass difference between 2002 and 2006, as exemplified by the small carbon source from the stand in the upper middle of the area (Fig. 12).

5. Discussion

5.1. Utility of multi-temporal lidar for monitoring forest ecosystems

Airborne lidar is well proven for measuring fine-scale vegetation attributes (Nelson, 2013). Its potential use for monitoring terrestrial environments has been growingly acknowledged and urged (Vierling et al., 2008). But the actual use of repeat lidar surveys to track ecosystem dynamics remains inadequately explored. Existing studies mostly analyzed single-time lidar data or used bi-temporal data to measure forest change at grid levels (Andersen et al., 2014; Cao et al., 2016; Dubayah et al., 2010; Hudak et al., 2012; Skowronski et al., 2014). Our work went further to consider four points in time and derive trajectories of multiple forest attributes at both individual trees and grid levels, describing exemplary methods well suited for repeat lidar data analyses and offering new empirical evidence that attests the utility of lidar for environmental monitoring and carbon management. Multi-level lidar dynamics information, such as that illustrated in Figs. 6 and 8, represents value-added products to support management, conservation, and research activities.

Individual tree dynamics information like ours can augment or even replace field surveys to study forest ecology and inform stand management. Indeed, an initial motivation for our repeat lidar surveys was to understand crown plastic responses to disturbances in hopes to improve timber quality and tree stability (Suarez-Minguez, 2010). In a tropical forest, the use of single-time lidar alone shed light on canopy gap dynamics (Asner et al., 2013). Such ecological understandings will be further advanced with multitemporal lidar. Ma et al. (2017), for example, derived 114,000 trees from bi-temporal lidar data to identify ecological controls on tree competition. Beyond individual tree levels, repeat lidar data capture 3D canopy dynamics and carbon flux at fine resolutions, helping to meet longstanding demands on reliable time-series data of ecosystem structure, especially for use in resource monitoring and terrestrial modeling (Goetz et al., 2015; Schimel et al., 2015). Many modelers believe that a true predictive science of biosphere won't be established until terrestrial models are constrained and evaluated using continuous high-quality ecological observations, such as those from multitemporal lidar (Hurtt et al., 2004; Moorcroft, 2006). These demonstrated and perceived values of vegetation dynamics information provide the impetus to motivate future multitemporal lidar studies and applications across scales.

5.2. Individual tree analysis

Lidar is deemed as the most promising tool to remotely map individual trees. Lidar-measured tree heights often fall within 2 m of field measurements after correction for the pulse density effect (e.g., RMSE = 0.11 m in our case) (Kwak et al., 2007; Suárez et al., 2005). Some practitioners note that lidar measures tree height better than field surveys (Sibona et al., 2016). Then, how well can lidar measure individual tree growth over time? The answer is case-specific, depending on lidar data quality and forest conditions. Our repeat lidar could detect growth of individual conifer trees as small as 0.24 m/year, as contrasted to 0.8 m/yr reported for a mixed-conifer forest in the US (Hudak et al., 2012) and 0.5 m/yr for a red pine planation in Canada (Hopkinson et al., 2008). Based on the respective growth rates, these detection limits indicate that repeat lidar could measure individual tree growth at intervals of < 3 years (e.g., half year in our case). This capability greatly complements and augments traditional periodic tree surveys (e.g., in a cycle of 5 years for the forest inventory program in the US).

Lidar detection of tree growth, however, is complicated and confounded by extraneous variations. Special care is needed to suppress the extraneous effects so as to reveal the true inherent dynamics (Hirata, 2004; Næsset, 2009). In the same way that satellite imagery requires correction for extraneous factors (Roy et al., 2016), repeat lidar data should be processed into standardized products that are consistent over time and amenable to inter-comparison (Hopkinson et al., 2013); CHM is one such product. But unlike the use of the same senor to acquire satellite data, repeat lidar data may come from sources that differ in sensor type, flight setting, waveform processing, and sampling density (Næsset, 2009; Roussel et al., 2017). The effect of lidar point density on individual tree analyses was found particularly strong. Lidar underestimates tree height more severely at lower point densities, attributed to higher chances of missing treetops or the DEM overestimation due to lower likelihoods to find true ground points (Gatziolis et al., 2010; Meng et al., 2010). This effect diminishes only if the point density is high enough (e.g., 7 pts/m^2 for our data). In general, density-dependent biases must be removed in order to confidently track individual tree growth.

Uncertainties associated with field data also cofound individual tree analyses (Popescu and Zhao, 2008). As in this study, tree parameters, such as height and locations, were difficult to measure with absolute accuracies in-situ, especially for closed canopies (Gatziolis et al., 2010). Unknown errors also arose from inconsistencies among field crew. Thus, observed deviations of lidar from field height, especially for our 2006 lidar data with 20 pts/m^2, may be dominated not by true lidar errors but rather by field measurement errors (Sibona et al., 2016). This speculation is warranted given the previously reported good results with high-density lidar data and the difficulty we experienced in measuring trees in situ (Yin and Wang, 2016). Definitive accuracy assessments of lidar height or other parameters need high-fidelity field data—a task infeasible for most applications due to logistical challenges (Gatziolis et al., 2010). Moreover, the field-to-lidar tree matching was made difficult by tree location errors and a lack of field-delineated crown data (Ayrey et al., 2017). Our matching algorithm alleviated this difficulty to some degree but suffered high commission error rates. A fully automatic, robust, accurate matching algorithm is desired but seems to not yet exist.

How to best achieve the potential of repeat lidar for automatic mapping of individual trees is still an open question. Despite two decades of lidar individual tree research (including this one), no tree detection algorithms are universally accepted as the standard or the best (Li et al., 2012; Popescu et al., 2003). To a lesser extent, even the automatic matching between lidar and field trees is challenging, as discussed above. A general lesson is that sophisticated algorithms, after intensive fine-tuning, may work well for some data and forest conditions but their transfer and implementation for other scenarios are not always feasible (Popescu and Zhao, 2008; Yin and Wang, 2016). In this regard, we made no attempt to build complex algorithms tailored to our data but instead, manually removed the algorithmic errors—a tedious but effective strategy enabling us to assess lidar accuracies based on only those trees correctly detected and matched. Meanwhile, our observation is that the relative community interest in improving lidar individual tree algorithms seems dampening. We hope that the potential and challenges identified here would spur new efforts on automatic lidar individual tree analyses, especially in the context of tracking forest changes over time.

5.3. Biomass dynamics and carbon flux

Lidar is also deemed by many practitioners as the most accurate tool to map forest structure and biomass. Our best biomass prediction accuracy was 14.7 Mg/ha ($RMSE_{CV}$) and 11.6% (relative error), meeting the requirement for operational carbon measurement, reporting, and verification activities (Zolkos et al., 2013). Over time, our lidar data could detect biomass change as small as 5 Mg/ha/year at a plot. Moreover, compared to individual tree analyses, the use of repeat lidar to measure biomass dynamics at the plot level is less affected by data inconsistency (Cao et al., 2016; Garcia et al., 2017b). In particular, the effect of lidar sampling density—a four-fold difference between our 2002 and 2006 data—was less pronounced or nonexistent. Hudak et al.

(2012) found that even a 30-fold difference in point density didn't affect plot-level biomass estimation. This insensitivity can be explained by likening the lidar scanning to the sampling from a probability distribution. Sampling tends to miss extreme values (e.g., local maxima denoting treetops) unless at very high sampling densities but gives reliable estimates of parameters (i.e., lidar metrics) insensitive to the sampling density. In addition, the inconsistency in repeat lidar data can be implicitly counteracted by the calibration of separate lidar models for different acquisition years with temporally-coincident ground biomass data.

Accuracies in lidar biomass estimates are constrained not just by lidar itself but also by the nature and quality of field data (Englhart et al., 2013). Uncertainties associated with field data, such as inaccurate allometry, measurement biases, and sampling errors, will be propagated through the modeling process, limiting the accuracies achievable irrespective of how perfectly a statistical model is fitted (Dubayah et al., 2010; Zolkos et al., 2013). Assessment of the true uncertainties therefore is difficult unless high-fidelity data such as those from destructive sampling are available—a practical paradox facing the validation of lidar approaches. Of particular note, the allometry we used refers to whole-tree biomass and may result in overestimation of carbon loss: Disturbed or cleared forests lose stems but may retain roots, but our models always account for the losses of both. Therefore, the interpretations of lidar-derived biomass change and carbon flux need extra care, especially if below-ground components are involved. Generally speaking, lidar-derived carbon fluxes are indicative of long-term carbon balance in a forest, but they differ fundamentally from those measured by eddy-covariance techniques (Baldocchi, 2003). The two are complementary and shouldn't be directly compared.

Three specific caveats are noted regarding our results and the general use of lidar for monitoring biomass and carbon. First, scales matter. RMSEs or absolute errors of biomass density estimates will decrease if spatially aggregated upward, a well-known statistical phenomenon independent of lidar or remote sensing data themselves (Zolkos et al., 2013). In our results, the measurable limit of 5 Mg/ha/year connotes an inability of lidar to detect any biomass change smaller than 5 Mg/ha/yr on a 25 m × 25 m grid, not contradicting our reported ability to detect an overall change of 1.2 Mg/ha/yr for the entire region—much larger than a grid/plot. Second, spatial autocorrelation in biomass estimates is widely acknowledged (Babcock et al., 2015). Additionally, our results suggest a potential temporal autocorrelation, especially for those undisturbed forests that accumulate biomass gradually. Its exact magnitude is not examined here, which will require advanced statistical inference to additionally estimate covariance of temporal correlation. Consideration of such temporal autocorrelation, therefore, will represent an opportunity to further improve the accuracy and robustness of lidar for monitoring biomass dynamics.

As a third caveat, the effectiveness of lidar to measure change is asymmetric with respect to the sign of the change. Tree losses tend to be more easily detectable than growth. Often, biomass losses are large in magnitude and abrupt whereas gains are small and incremental. As a result, field-measured biomass loss and gain can show differing error characteristics (Fig. 11), thus making it inappropriate to calibrate regression models to such field data assuming homogenous errors. This asymmetry can explain why our direct method to estimate biomass change was poorer (Fig. 11): Large biomass losses of disturbed plots can dwarf small, incremental gains of the many undisturbed plots and therefore become high-leverage points in the regression (Fig. 11), misleading the fitting of the direct-method model. We therefore expect that if field plots have moderate biomass losses or if all the plots have biomass gains, the direct method of estimating biomass change is more likely to perform better than the indirect method. This reasoning provides a plausible explanation on the conflicting results about relative accuracies of indirect and direct methods in earlier lidar biomass change studies (Cao et al., 2016). Irrespectively, the asymmetry identified here should be leveraged to improve modeling, for example, by fitting lidar models to biomass gain and loss separately or accounting for heterogeneous errors in field-measured biomass change explicitly—some strategies to be tested in future research.

Recent years see an increasing interest in seeking lidar-based biomass models that are universal and transferable, in part to mitigate the lack of field data for model calibration in regional mapping (Asner et al., 2012b). Our linear functional model provides one such viable candidate. Its generality and transferability do not preclude the need for ground data but do lessen the reliance on temporally-concomitant field-based biomass for calibrating historical lidar data. This property is particularly attractive, given that no field data can be collected retrospectively. In contrast, random forests or machine learning models are blackboxes, often lacking transferability and unlikely uncovering the true or a physically-sound predictive relationship (Liang, 2007; Zhao et al., 2013). As with our linear model, the true lidar-biomass relationship is more likely to be inferred by resorting to first principles and remote sensing physics (Liang, 2007; Zhao et al., 2015). Our linear model was tested first for a US temperate forest in Zhao et al. (2009) and for a second time here, both showing good predictive power and model generality. We encourage researchers to further test its utility and validity over forests in other biomes. Furthermore, decades of lessons on optical remote sensing somehow indicate that calibrated empirical models with true universal applicability are unlikely to exist (Liang, 2007; Lu, 2006; Zhao et al., 2013) and that model transferability should be interpreted relatively, subject to modelers' tolerance of allowable errors (Schweiger et al., 2015).

Is our linear functional model better than random forests? Unarguably, random forests is powerful for empirical modeling on complex data (Friedman et al., 2001). Its demonstrated predictive power for biomass, however, was poorer than the linear model, highlighting the strengths of mechanistic models over pure empirical models. In theory, there are infinite ways of modeling: Numerous ways are possible to compute lidar metrics, select predictors, choose modeling techniques, formulate equation forms, and determine calibration strategies, among others (Næsset et al., 2005; Zhao et al., 2013). Practitioners examine only a finite set of candidate models (Hultquist et al., 2014; Zhao et al., 2013), a process informed by theoretical and experimental evidence as well as by modelers' knowledge and philosophy. The searching for the so-called “best” or a “better” model should always be understood as relative and scenario-specific (Friedman et al., 2001; Jensen, 1986; Zolkos et al., 2013). As much, the emphasis of our model evaluation is not on despising or advocating one against another for future studies but rather testing models' behavior and generality in a particular case study.

We believe that the use of lidar for ecosystem studies is both a science and an art (Jensen, 1986). Development of lidar methods involves many subjective factors (Zhao et al., 2013), as hinted by our preference of certain tree delineation rules and regression models. Given the same task, analysts act differently for idiosyncratic reasons (Friedman et al., 2001; Hultquist et al., 2014): Some lidar practitioners prefer individual tree to area-based approaches, conventional regression to machine learning, model-based to designed-based inference, or mean height to quartile height as predictor. Even what is known as standard may be handled differently. For instance, common lidar products or metrics, such as CHM and quantile heights, have been derived in different fashions, regarding data pre-processing, types of lidar points used, filtering methods, interpolation, and post-processing (Zhao and Popescu, 2007). Regression modeling is another process fraught with numerous options (Zhao et al., 2013). Given the same predictors, analysts calibrate linear models differently: partial or ordinary least squares; Bayesian inference; or L1 and ridge regression (Næsset et al., 2005; Zhao et al., 2013). Which is a better method to map ecosystem structure and dynamics with lidar is both a technical issue and a subjective matter.

5.4. Looking forward

The future use of multitemporal lidar embraces both prospects and challenges. Lidar technologies are mature enough (Shan and Toth, 2008) and data costs are declining — £6.5 per ha in 2002 and £1.0 per ha in 2012 in our case. The role of lidar as a multi-purpose tool is growingly recognized by multiple interested parties; partnerships among federal, state, local, commercial or academic players have become an important business model for seamless lidar data collection (Stoker et al., 2008). Many institutions even have their own lidar systems dedicated to ecosystem research, such as NASA's G-LiHT, Stanford's CAO, NEON's AOP, and Chinese Academy of Forestry's LiCHy (Asner et al., 2012a; Cook et al., 2013; Kampe et al., 2010; Pang et al., 2016). Despite the declining costs and increasing data availability, lidar currently is not affordable enough to be deployed frequently over extensive areas; airborne laser scanning data overall are still limited in coverage and repeatability. Therefore, any existing lidar data, including those acquired for purposes other than ecosystem studies, will be valuable in serving baseline data for future monitoring activities and change analyses (Jackson, 2002). Meanwhile, ancillary ground data are needed to maximize lidar utility (Næsset et al., 2005), which, if not available, constitute another limiting factor.

Accompanying the growing use of airborne lidar is an intensified interest in applying multispectral time-series imagery to study ecosystem dynamics (Goetz et al., 2006), attributed to increased data availability such as opening of Landsat archives and growth of UAV systems (Wulder et al., 2012). Despite the superiority of lidar for ecosystem studies, no technology will replace the other. Rather, they complement each other and should be integrated (Sankey and Glenn, 2011). In particular, the forest change trajectories we derived depict decadal trends and cannot resolve short-term changes or transient disturbances. The low temporal resolution of repeat lidar data is also a problem for many practical applications and can be alleviated by fusing satellite data to leverage the time-resolved capability of satellite imagery and the rich spatial details of lidar point clouds (Ahmed et al., 2015; Garcia et al., 2017a). Data fusion also helps to mitigate the problems associated with limited lidar coverage, as exemplified in the use of lidar as a sampling tool to calibrate satellite data for regional carbon mapping. Given these benefits, it is not a surprise that the future will see a rise in the integration of multitemporal lidar and satellite data to map land surface changes and forest dynamics.

Multitemporal lidar adds the time dimension to 3D xyz data and may be further augmented with the fifth dimension—intensity or spectra (Eitel et al., 2016). The prospect of capturing snapshots of landscapes permanently in 3D point clouds is exciting, offering attractive solutions to probing environment changes and processes with levels of spatial details and accuracies unattainable by other remote sensing technologies — a capability exemplified and expanded by our lidar analyses. However, this capability may not automatically manifest itself as true utility to end users (Gibbs et al., 2007; Kalluri et al., 2003). The technical intricacies of many lidar vegetation analyses may bewilder experts let alone stakeholders. To accelerate the credible use of lidar, participatory modeling approaches can be employed to engage stakeholders in learning the strengths and weaknesses of lidar products and accordingly, to boost their trustworthiness and confidence in adopting lidar products for critical applications such as conservation and carbon trading (Mendoza and Prabhu, 2005; Sandker et al., 2010). Nonetheless, the future use of multitemporal lidar is bright.

6. Summary

Lidar boasts the best technology for mapping 3D vegetation structure; its utility for tackling forest dynamics over time at fine scales was assessed and confirmed by our individual tree and grid-level analyses. Our analyses imply that lidar could confidently detect individual tree growth at sub-annual intervals, but this ability depends on lidar sampling rates: At lower sampling rates, lidar is more likely to miss treetop and underestimate tree height. Such biases have to be removed for reliably deriving tree growth from repeat data of varying point density. At grid/plot levels, estimation of biomass over time was affected not much by extraneous variation in repeat lidar data but greatly by model choices. Our semi-mechanistic linear model outcompeted Random Forests. This shouldn't be misconstrued as our discouraging the use of machine learning. Rather, we hope that the generality of our linear model will inspire more efforts in applying remote sensing physics to inform lidar biomass estimation. Physically-based models like ours mitigate the reliance on ground data for model calibration, offering possibilities to leverage historical lidar data even if no concomitant field data exist. Overall, the utility of multitemporal lidar for ecological and environmental monitoring is enormous and is expected to be further augmented through the integration of satellite time-series data. We envision an ever-increasing role of lidar in supporting research and management activities, such as those concerning carbon sciences, forest degradation, biodiversity conservation, and land-use.

Acknowledgements

This work was supported by the Open Research Fund from the State Key Laboratory of Digital Earth Science, Institute of Remote Sensing and Digital Earth, Chinese Academy of Sciences (OFSLRSS201604); a Microsoft Azure Research Award (CRM:0518513); and the Marie Curie International Outgoing Fellowship within the 7th European Community Framework Programme (ForeStMap—3D Forest Structure Monitoring and Mapping, Project Reference: 629376). The contents of this paper reflect solely the authors' views and not those of the European Commission. We thank Xiaohuan Xi, Erik Nasset, Bruce Cook, Greg Asner, Yong Pang, Qinghua Guo, Dan Liu, Haiming Qin, Sarah Barbee, and Shu Liu for their help of various forms with this work and this manuscript. Special thanks go to Ross Nelson, Shruthi Srinivasan, and two reviewers for their detailed comments that improved this manuscript.

References

Ahmed, O.S., Franklin, S.E., Wulder, M.A., White, J.C., 2015. Characterizing stand-level forest canopy cover and height using landsat time series, samples of airborne LiDAR, and the random forest algorithm. ISPRS J. Photogramm. Remote Sens. 101, 89–101.

Andersen, H.-E., Reutebuch, S.E., McGaughey, R.J., d'Oliveira, M.V., Keller, M., 2014. Monitoring selective logging in western Amazonia with repeat lidar flights. Remote Sens. Environ. 151, 157–165.

Asner, G.P., Knapp, D.E., Boardman, J., Green, R.O., Kennedy-Bowdoin, T., Eastwood, M., Martin, R.E., Anderson, C., Field, C.B., 2012a. Carnegie Airborne Observatory-2: increasing science data dimensionality via high-fidelity multi-sensor fusion. Remote Sens. Environ. 124, 454–465.

Asner, G.P., Mascaro, J., Muller-Landau, H.C., Vieilledent, G., Vaudry, R., Rasamoelina, M., Hall, J.S., van Breugel, M., 2012b. A universal airborne LiDAR approach for tropical forest carbon mapping. Oecologia 168, 1147–1160.

Asner, G.P., Kellner, J.R., Kennedy-Bowdoin, T., Knapp, D.E., Anderson, C., Martin, R.E., 2013. Forest canopy gap distributions in the southern Peruvian Amazon. PLoS One 8, e60875.

Axelsson, P., 2000. DEM generation from laser scanner data using adaptive TIN models. Int. Arch. Photogramm. Remote. Sens. 33, 111–118.

Ayrey, E., Fraver, S., Kershaw Jr., J.A., Kenefic, L.S., Hayes, D., Weiskittel, A.R., Roth, B.E., 2017. Layer stacking: a novel algorithm for individual forest tree segmentation from LiDAR point clouds. Can. J. Remote. Sens. 1–13.

Babcock, C., Finley, A.O., Bradford, J.B., Kolka, R., Birdsey, R., Ryan, M.G., 2015. LiDAR based prediction of forest biomass using hierarchical models with spatially varying coefficients. Remote Sens. Environ. 169, 113–127.

Baldocchi, D.D., 2003. Assessing the eddy covariance technique for evaluating carbon dioxide exchange rates of ecosystems: past, present and future. Glob. Chang. Biol. 9, 479–492.

Bonan, G.B., 2008. Forests and climate change: forcings, feedbacks, and the climate benefits of forests. Science 320, 1444–1449.

Cao, L., Coops, N.C., Innes, J.L., Sheppard, S.R., Fu, L., Ruan, H., She, G., 2016. Estimation of forest biomass dynamics in subtropical forests using multi-temporal airborne LiDAR data. Remote Sens. Environ. 178, 158–171.

Cook, B.D., Nelson, R.F., Middleton, E.M., Morton, D.C., McCorkel, J.T., Masek, J.G., Ranson, K.J., Ly, V., Montesano, P.M., 2013. NASA Goddard's LiDAR, hyperspectral and thermal (G-LiHT) airborne imager. Remote Sens. 5, 4045–4066.

Coomes, D.A., Dalponte, M., Jucker, T., Asner, G.P., Banin, L.F., Burslem, D.F., Lewis, S.L.,

Nilus, R., Phillips, O.L., Phua, M.-H., 2017. Area-based vs tree-centric approaches to mapping forest carbon in Southeast Asian forests from airborne laser scanning data. Remote Sens. Environ. 194, 77–88.
Dassot, M., Constant, T., Fournier, M., 2011. The use of terrestrial LiDAR technology in forest science: application fields, benefits and challenges. Ann. For. Sci. 68, 959–974.
DeVries, B., Verbesselt, J., Kooistra, L., Herold, M., 2015. Robust monitoring of small-scale forest disturbances in a tropical montane forest using Landsat time series. Remote Sens. Environ. 161, 107–121.
Dubayah, R.O., Drake, J.B., 2000. Lidar remote sensing for forestry. J. For. 98, 44–46.
Dubayah, R., Sheldon, S., Clark, D., Hofton, M., Blair, J., Hurtt, G., Chazdon, R., 2010. Estimation of tropical forest height and biomass dynamics using lidar remote sensing at La Selva, Costa Rica. J. Geophys. Res. Biogeosci. 115.
Eitel, J.U., Höfle, B., Vierling, L.A., Abellán, A., Asner, G.P., Deems, J.S., Glennie, C.L., Joerg, P.C., LeWinter, A.L., Magney, T.S., 2016. Beyond 3-D: the new spectrum of lidar applications for earth and ecological sciences. Remote Sens. Environ. 186, 372–392.
Englhart, S., Jubanski, J., Siegert, F., 2013. Quantifying dynamics in tropical peat swamp forest biomass with multi-temporal LiDAR datasets. Remote Sens. 5, 2368–2388.
Foody, G.M., Boyd, D.S., Cutler, M.E., 2003. Predictive relations of tropical forest biomass from Landsat TM data and their transferability between regions. Remote Sens. Environ. 85, 463–474.
Friedman, J., Hastie, T., Tibshirani, R., 2001. The elements of statistical learning. In: Springer Series in Statistics Springer, Berlin.
García, M., Popescu, S., Riaño, D., Zhao, K., Neuenschwander, A., Agca, M., Chuvieco, E., 2012. Characterization of canopy fuels using ICESat/GLAS data. Remote Sens. Environ. 123, 81–89.
García, M., Gajardo, J., Riaño, D., Zhao, K., Martín, P., Ustin, S., 2015. Canopy clumping appraisal using terrestrial and airborne laser scanning. Remote Sens. Environ. 161, 78–88.
Garcia, M., Saatchi, S., Casas, A., Koltunov, A., Ustin, S., Ramirez, C., Garcia-Gutierrez, J., Balzter, H., 2017a. Quantifying biomass consumption and carbon release from the California Rim fire by integrating airborne LiDAR and Landsat OLI data. J. Geophys. Res. Biogeosci. 122, 340–353.
Garcia, M., Saatchi, S., Ferraz, A., Silva, C.A., Ustin, S., Koltunov, A., Balzter, H., 2017b. Impact of data model and point density on aboveground forest biomass estimation from airborne LiDAR. Carbon Balance Manag. 12, 4.
Gatziolis, D., Fried, J.S., Monleon, V.S., 2010. Challenges to estimating tree height via LiDAR in closed-canopy forests: a parable from western Oregon. For. Sci. 56, 139–155.
Gibbs, H.K., Brown, S., Niles, J.O., Foley, J.A., 2007. Monitoring and estimating tropical forest carbon stocks: making REDD a reality. Environ. Res. Lett. 2, 045023.
Goetz, S.J., Fiske, G.J., Bunn, A.G., 2006. Using satellite time-series data sets to analyze fire disturbance and forest recovery across Canada. Remote Sens. Environ. 101, 352–365.
Goetz, S.J., Steinberg, D., Betts, M.G., Holmes, R.T., Doran, P.J., Dubayah, R., Hofton, M., 2010. Lidar remote sensing variables predict breeding habitat of a Neotropical migrant bird. Ecology 91, 1569–1576.
Goetz, S.J., Hansen, M., Houghton, R.A., Walker, W., Laporte, N., Busch, J., 2015. Measurement and monitoring needs, capabilities and potential for addressing reduced emissions from deforestation and forest degradation under REDD +. Environ. Res. Lett. 10, 123001.
Green, C., Tobin, B., O'Shea, M., Farrell, E.P., Byrne, K.A., 2007. Above-and belowground biomass measurements in an unthinned stand of Sitka spruce (*Picea sitchensis* (Bong) Carr.). Eur. J. For. Res. 126, 179–188.
Hirata, Y., 2004. The Effects of Footprint Size and Sampling Density in Airborne Laser Scanning to Extract Individual Trees in Mountainous Terrain. 8. SPRS working group, pp. 102–107.
Hopkinson, C., Chasmer, L., Hall, R., 2008. The uncertainty in conifer plantation growth prediction from multi-temporal lidar datasets. Remote Sens. Environ. 112, 1168–1180.
Hopkinson, C., Chasmer, L., Colville, D., Fournier, R.A., Hall, R.J., Luther, J.E., Milne, T., Petrone, R.M., St-Onge, B., 2013. Moving toward consistent ALS monitoring of forest attributes across Canada. Photogramm. Eng. Remote. Sens. 79, 159–173.
Hudak, A.T., Strand, E.K., Vierling, L.A., Byrne, J.C., Eitel, J.U., Martinuzzi, S., Falkowski, M.J., 2012. Quantifying aboveground forest carbon pools and fluxes from repeat LiDAR surveys. Remote Sens. Environ. 123, 25–40.
Hultquist, C., Chen, G., Zhao, K., 2014. A comparison of Gaussian process regression, random forests and support vector regression for burn severity assessment in diseased forests. Remote Sens. Lett. 5, 723–732.
Hurtt, G.C., Dubayah, R., Drake, J., Moorcroft, P.R., Pacala, S.W., Blair, J.B., Fearon, M.G., 2004. Beyond potential vegetation: combining lidar data and a height-structured model for carbon studies. Ecol. Appl. 14, 873–883.
Jackson, R., 2002. The Earth Remains Forever: Generations at a Crossroads. University of Texas Press.
Jensen, J.R., 1986. Introductory Digital Image Processing: A Remote Sensing Perspective. Univ. of South Carolina, Columbus.
Kalluri, S., Gilruth, P., Bergman, R., 2003. The potential of remote sensing data for decision makers at the state, local and tribal level: experiences from NASA's synergy program. Environ. Sci. Pol. 6, 487–500.
Kampe, T.U., Johnson, B.R., Kuester, M., Keller, M., 2010. NEON: the first continental-scale ecological observatory with airborne remote sensing of vegetation canopy biochemistry and structure. J. Appl. Remote. Sens. 4, 043510-043510-043524.
Kwak, D.-A., Lee, W.-K., Lee, J.-H., Biging, G.S., Gong, P., 2007. Detection of individual trees and estimation of tree height using LiDAR data. J. For. Res. 12, 425–434.
Li, W., Guo, Q., Jakubowski, M.K., Kelly, M., 2012. A new method for segmenting individual trees from the lidar point cloud. Photogramm. Eng. Remote. Sens. 78, 75–84.
Liang, S., 2007. Recent developments in estimating land surface biogeophysical variables from optical remote sensing. Prog. Phys. Geogr. 31, 501–516.
Lu, D., 2006. The potential and challenge of remote sensing-based biomass estimation. Int. J. Remote Sens. 27, 1297–1328.
Ma, Q., Su, Y., Tao, S., Guo, Q., 2017. Quantifying individual tree growth and tree competition using bi-temporal airborne laser scanning data: a case study in the Sierra Nevada Mountains, California. Int. J. Digital Earth 1–19.
Magnussen, S., Næsset, E., Kändler, G., Adler, P., Renaud, J., Gobakken, T., 2016. A functional regression model for inventories supported by aerial laser scanner data or photogrammetric point clouds. Remote Sens. Environ. 184, 496–505.
May, N.C., Toth, C.K., 2007. Point positioning accuracy of airborne LiDAR systems: A rigorous analysis. Int. Arch. Photogramm. Remote. Sens. Spat. Inf. Sci. 36, 107–111 (no. 3/W49B, Sep.).
Mendoza, G.A., Prabhu, R., 2005. Combining participatory modeling and multi-criteria analysis for community-based forest management. For. Ecol. Manag. 207, 145–156.
Meng, X., Currit, N., Zhao, K., 2010. Ground filtering algorithms for airborne LiDAR data: a review of critical issues. Remote Sens. 2, 833–860.
Moorcroft, P.R., 2006. How close are we to a predictive science of the biosphere? Trends Ecol. Evol. 21, 400–407.
Mutlu, M., Popescu, S.C., Zhao, K., 2008. Sensitivity analysis of fire behavior modeling with LIDAR-derived surface fuel maps. For. Ecol. Manag. 256, 289–294.
Muukkonen, P., 2007. Generalized allometric volume and biomass equations for some tree species in Europe. Eur. J. For. Res. 126, 157–166.
Næsset, E., 2009. Effects of different sensors, flying altitudes, and pulse repetition frequencies on forest canopy metrics and biophysical stand properties derived from small-footprint airborne laser data. Remote Sens. Environ. 113, 148–159.
Næsset, E., Bollandsås, O.M., Gobakken, T., 2005. Comparing regression methods in estimation of biophysical properties of forest stands from two different inventories using laser scanner data. Remote Sens. Environ. 94, 541–553.
Nelson, R., 2013. How did we get here? An early history of forestry lidar1. Can. J. Remote. Sens. 39, S6–S17.
Nunes, M.H., Ewers, R.M., Turner, E.C., Coomes, D.A., 2017. Mapping aboveground carbon in oil palm plantations using LiDAR: a comparison of tree-centric versus area-based approaches. Remote Sens. 9, 816.
Palace, M.W., Sullivan, F.B., Ducey, M.J., Treuhaft, R.N., Herrick, C., Shimbo, J.Z., Mota-E-Silva, J., 2015. Estimating forest structure in a tropical forest using field measurements, a synthetic model and discrete return lidar data. Remote Sens. Environ. 161, 1–11.
Pang, Y., Li, Z., Ju, H., Lu, H., Jia, W., Si, L., Guo, Y., Liu, Q., Li, S., Liu, L., 2016. LiCHy: the CAF's LiDAR, CCD and hyperspectral integrated airborne observation system. Remote Sens. 8, 398.
Popescu, S.C., Zhao, K., 2008. A voxel-based lidar method for estimating crown base height for deciduous and pine trees. Remote Sens. Environ. 112, 767–781.
Popescu, S.C., Wynne, R.H., Nelson, R.F., 2003. Measuring individual tree crown diameter with lidar and assessing its influence on estimating forest volume and biomass. Can. J. Remote. Sens. 29, 564–577.
Réjou-Méchain, M., Tymen, B., Blanc, L., Fauset, S., Feldpausch, T.R., Monteagudo, A., Phillips, O.L., Richard, H., Chave, J., 2015. Using repeated small-footprint LiDAR acquisitions to infer spatial and temporal variations of a high-biomass Neotropical forest. Remote Sens. Environ. 169, 93–101.
Roussel, J.-R., Caspersen, J., Béland, M., Thomas, S., Achim, A., 2017. Removing bias from LiDAR-based estimates of canopy height: accounting for the effects of pulse density and footprint size. Remote Sens. Environ. 198, 1–16.
Roy, D., Zhang, H., Ju, J., Gomez-Dans, J., Lewis, P., Schaaf, C., Sun, Q., Li, J., Huang, H., Kovalskyy, V., 2016. A general method to normalize Landsat reflectance data to nadir BRDF adjusted reflectance. Remote Sens. Environ. 176, 255–271.
Sandker, M., Campbell, B., Ruiz-Pérez, M., Sayer, J., Cowling, R., Kassa, H., Knight, A., 2010. The role of participatory modeling in landscape approaches to reconcile conservation and development. Ecol. Soc. 15.
Sankey, T., Glenn, N., 2011. Landsat-5 TM and lidar fusion for sub-pixel juniper tree cover estimates in a western rangeland. Photogramm. Eng. Remote. Sens. 77, 1241–1248.
Schimel, D., Pavlick, R., Fisher, J.B., Asner, G.P., Saatchi, S., Townsend, P., Miller, C., Frankenberg, C., Hibbard, K., Cox, P., 2015. Observing terrestrial ecosystems and the carbon cycle from space. Glob. Chang. Biol. 21, 1762–1776.
Schweiger, A.K., Risch, A.C., Damm, A., Kneubühler, M., Haller, R., Schaepman, M.E., Schütz, M., 2015. Using imaging spectroscopy to predict above-ground plant biomass in alpine grasslands grazed by large ungulates. J. Veg. Sci. 26, 175–190.
Shan, J., Toth, C.K., 2008. Topographic Laser Ranging and Scanning: Principles and Processing. CRC press.
Sibona, E., Vitali, A., Meloni, F., Caffo, L., Dotta, A., Lingua, E., Motta, R., Garbarino, M., 2016. Direct measurement of tree height provides different results on the assessment of LiDAR accuracy. Forests 8, 7.
Skowronski, N.S., Clark, K.L., Gallagher, M., Birdsey, R.A., Hom, J.L., 2014. Airborne laser scanner-assisted estimation of aboveground biomass change in a temperate oak–pine forest. Remote Sens. Environ. 151, 166–174.
Srinivasan, S., Popescu, S.C., Eriksson, M., Sheridan, R.D., Ku, N.-W., 2014. Multi-temporal terrestrial laser scanning for modeling tree biomass change. For. Ecol. Manag. 318, 304–317.
Ståhl, G., Heikkinen, J., Petersson, H., Repola, J., Holm, S., 2014. Sample-based estimation of greenhouse gas emissions from forests—a new approach to account for both sampling and model errors. For. Sci. 60, 3–13.
Stoker, J.M., Harding, D., Parrish, J., 2008. The need for a national LIDAR dataset. Photogramm. Eng. Remote. Sens. 74, 1066–1068.
Suárez, J.C., Ontiveros, C., Smith, S., Snape, S., 2005. Use of airborne LiDAR and aerial photography in the estimation of individual tree heights in forestry. Comput. Geosci. 31, 253–262.

Suarez-Minguez, J.C., 2010. An Analysis of the Consequences of Stand Variability in Sitka Spruce Plantations in Britain Using a Combination of Airborne LiDAR Analysis and Models. The University of Sheffield.
Thomas, V., Treitz, P., McCaughey, J., Morrison, I., 2006. Mapping stand-level forest biophysical variables for a mixedwood boreal forest using lidar: an examination of scanning density. Can. J. For. Res. 36, 34–47.
Véga, C., Renaud, J.-P., Durrieu, S., Bouvier, M., 2016. On the interest of penetration depth, canopy area and volume metrics to improve Lidar-based models of forest parameters. Remote Sens. Environ. 175, 32–42.
Vierling, K.T., Vierling, L.A., Gould, W.A., Martinuzzi, S., Clawges, R.M., 2008. Lidar: shedding new light on habitat characterization and modeling. Front. Ecol. Environ. 6, 90–98.
West, P.W., West, P.W., 2009. Tree and Forest Measurement. Springer.
Wulder, M.A., Masek, J.G., Cohen, W.B., Loveland, T.R., Woodcock, C.E., 2012. Opening the archive: how free data has enabled the science and monitoring promise of Landsat. Remote Sens. Environ. 122, 2–10.
Yin, D., Wang, L., 2016. How to assess the accuracy of the individual tree-based forest inventory derived from remotely sensed data: a review. Int. J. Remote Sens. 37, 4521–4553.
Yu, X., Hyyppä, J., Kukko, A., Maltamo, M., Kaartinen, H., 2006. Change detection techniques for canopy height growth measurements using airborne laser scanner data. Photogramm. Eng. Remote. Sens. 72, 1339–1348.
Yu, X., Hyyppä, J., Vastaranta, M., Holopainen, M., Viitala, R., 2011. Predicting individual tree attributes from airborne laser point clouds based on the random forests technique. ISPRS J. Photogramm. Remote Sens. 66, 28–37.
Zhao, K., Jackson, R.B., 2014. Biophysical forcings of land-use changes from potential forestry activities in North America. Ecol. Monogr. 84, 329–353.
Zhao, K., Popescu, S., 2007. In: Hierarchical watershed segmentation of canopy height model for multi-scale forest inventory. Proceedings of the ISPRS Working Group “Laser Scanning”. pp. 436–442.
Zhao, K., Popescu, S., Nelson, R., 2009. Lidar remote sensing of forest biomass: a scale-invariant estimation approach using airborne lasers. Remote Sens. Environ. 113, 182–196.
Zhao, K., Popescu, S., Meng, X., Pang, Y., Agca, M., 2011. Characterizing forest canopy structure with lidar composite metrics and machine learning. Remote Sens. Environ. 115, 1978–1996.
Zhao, K., Valle, D., Popescu, S., Zhang, X., Mallick, B., 2013. Hyperspectral remote sensing of plant biochemistry using Bayesian model averaging with variable and band selection. Remote Sens. Environ. 132, 102–119.
Zhao, K., García, M., Liu, S., Guo, Q., Chen, G., Zhang, X., Zhou, Y., Meng, X., 2015. Terrestrial lidar remote sensing of forests: maximum likelihood estimates of canopy profile, leaf area index, and leaf angle distribution. Agric. For. Meteorol. 209, 100–113.
Zolkos, S., Goetz, S., Dubayah, R., 2013. A meta-analysis of terrestrial aboveground biomass estimation using lidar remote sensing. Remote Sens. Environ. 128, 289–298.